Petrology and Geochemistry of Lavas and Pyroclastics

4

Volker Jörg Dietrich and Răzvan-Gabriel Popa

Abstract

This chapter offers a comprehensive overview of the main petrologic of geochemical characteristics of the Nisyros volcanic products, integrating published data and some new observations. The mineralogy and petrography of the magmatic rocks are described, including a brief presentation of enclaves, xenoliths and xenocrysts. The disequilibrium textures of amphibole are also presented, in light of the thermodynamic changes recorded by their breakdown structures and reaction rims. The chapter contains a holistic overview of the whole-rock major and trace element geochemistry of the rocks, obtained by compiling the available published data. Calc-alkaline and arc tholeiite trends are inferred, and the silica-gap is observable just before amphibole fractionation starts. A brief description of the main petrographic and geochemical features of each lithostratigraphic unit, according to the map, is offered. The chapter concludes with a discussion on the petrogenetic evolution of the island, including crustal assimilation, fractional crystallisation, magma mixing and mingling, crystal-retention-liquid-segregation, the probable depth of the magma chamber and models for generating the highly silicic magmas characteristic for the younger eruptive events, from the parental basaltic andesite melts that were erupted in the earlier stages.

Electronic supplementary material The online version of this chapter (doi:10.1007/978-3-319-55460-0_4) contains supplementary material, which is available to authorized users.

V.J. Dietrich (✉) · R.-G. Popa
Institute of Geochemistry and Petrology, Swiss Federal Institute of Technology, ETH Zurich, ETH-Zentrum, 8092 Zürich, Switzerland
e-mail: volker.dietrich@erdw.ethz.ch

R.-G. Popa
e-mail: razvan.popa@erdw.ethz.ch

4.1 Introduction

The volcanic products of Nisyros Island: lavas, domes and pyroclastic deposits, have compositions ranging from basaltic andesite to rhyolite and belong to the typical calc-alkaline island-arc magmatic series. In the past 50 years the mineralogy, petrography, geochemistry and isotope

V.J. Dietrich and E. Lagios (eds.), *Nisyros Volcano*, Active Volcanoes of the World,
DOI 10.1007/978-3-319-55460-0_4

Table 4.1 Summary of petrography and mineral content according to lithostratigraphic rock units

LSU	Eruption mode	Thickness (m)	Rocktype	special texture	Plagioclase	Clinopyrox.	Orthopyr.	Olivine	Amphibole	Biotite	Oxides	Apatite	Zircon	Sanidin*	Quartz	LSU
	Post-Caldera Eruptive Cycles															
32	Lava domes, flows	600	Rhyodacite	hypocryst. porph.	P15, M	P<5, M	P<5, M	TR (Fayal.)	P<5, RC		P<5			TR,Or70	TR	32
32	Enclaves			quenched, porphy.	P, M	M			P, M, RC							32
	Caldera Eruptive Cycles and Caldera Collapse															
31	Fl-WS-Fl-PbS-succ.	max. 30	Rhyolite	pumice, P.I. 10	P<5	P<5, M	P<5		P<5, RC		P<5	P<5	P<5			31
31	Enclaves			quenched, porphy.					P<M, RC							31
30	Lava flows	150	Rhyolite	hypocryst. porph.	P<5, M	P<5	P<5, M		P<5, M	TR	P<5			TR,Or54		30
30	Enclaves			quenched, porphy.	P, M	M			P, M, RC							30
28	F-Fl-WS-Fl-succ.	max. 20	Rhyolite	pumice, P.I. 5	P<5, M		P<5, M		TR, RC		P<5	P<5	P<5		TR	28
28	Enclaves			quenched, porphy.	P, M	M			P, M, RC							28
27	Lava flow	max. 10	Andesite	porph., P.I. 10-15	P<5, M	P<5, M		P<5			P<5, M					27
	Composite Stratovolcano Cycles															
26	Dome collapse breccia	20-30	Dacite	porph., P.I. 20-30	P5-10, M	P<5, M	P<5, M		P<5, RC	TR	P<5	P<5	P<5			26
26	Enclaves 1-2%		Andesite	quenched	P, M	P, M			P, M, RC							26
25	Flows, dome	150	Dacite	porph., P.I. 20-30	P5-10, M	P<5, M	P<5, M		P<5, PR, RC	TR	P<5, M	P<5	P<5	TR,Or42		25
25	Enclaves 1-2 %		Andesite	quenched	M				P, M, RC							25
24	Flows	max. 25	Bas. Andes.	glomeroporhyr.	P<5-15, M	P<5-10, M	M	P<5			P<5, M					24
22	Flows	max. 10	Bas. Andes.	glomeroporhyr.	P<5-20, M	P<5-10,AC, M	P<1	P<5			P<5, M					22
21	F-PbS-PyFl-succ.	max. 15	Bas. Andes.		P<5-10, M	P<5-10, M	P<1	P<5			P<5, M					21
19	F-S-F-3S-F-F-xS-F-succ.		Bas.And.- Dac.		P<5, M	P<5, M	P<5, M				P<5, M				TR	19
18	Lava flow	10 ?	Dacite	porph., P.I. 20-30	P10, M	P<5, M	P<5, M		P<5		P<5, M	P<5	P<5			18
17	Lava domes, flows	max. 60	Rhyolite	vitrophyr., perlitic	P<5-10,AC, M	P<5, M	P<5, M		P<5	M	P<5, M	P<5	P<5	M,TR	TR	17
16	S-Fl-succession	30	Bas. Andes.	porph., P.I. 20-30	P10	P<5	P<1	PR			P<5					16
15	Lava flow	max. 40	Andesite	glomeroporhyr.	P<5-10, AC, M	P<5, AC, M	P<1	P<5			P<5, M					15
14	Lava flow	max. 25	Dacite	porph., P.I. 20-30	P15, M	P<5, M	P<5, M	P<5	RC	TR	P<5, M	P<5				14
14	Enclaves up to 30%		Andesite	porp., quenched	P, M	P, M	P<1		P, M, RC							14
13	Lava flow	max. 40	Andesite	porph., P.I. 2-15	P<5-15, M	P<5-10, M	P<1	P<5, PR			P<5, M					13
	Early Shield Volcano Cycles of Nisyros															
11	F-Fl-F-S-Fl-succ.	35	Andesite		P5-20, AC, M	P<5, M	M	P<5, PR			P<5, M					11
10	Lava flows	70	Bas. Andes.	scoria-rich	P5->20, AC, M	P5-15, M	TR	P<5, PR			P<5, M					10
8	Lava flow	5	Bas. Andes.	porph., P.I. 40-50	P5-20,AC, M	P<5-15, M	TR	P<5-10			P<5, M					8
6	S-F-Fl-S-Fl-succ.	60	Bas. Andes.		P<5, M	P<5, M	TR	P<5	TR, RC		P<5, M					6
5	Lava flows	40	Andesite	glomeroporhyr.	P<5-15, M	P<5-10, M	P<5	PR			P<5, M					5
4	F-Fl-S-F-succ.	30	Andesite		P<5, M	P<5, M	P<1	P<5	TR, RC		P<5, M					4
3	Lava flow	35	Bas. Andes.	porph., P.I. 20-30	P10-20, AC,M	P10, M	TR	P<5			P<5, M					3
	Submarine volcanic base															
1,2	Pillow & lava flows	max.50 ?	Bas-Andes.	partly hyaloclast.	P10-20, AC,M	P10	TR	P<1	TR, RC		P<5, M					1,2

Phenocryst abundance in vol.% of total rock

P phenocryst, *P < 1* max. 1 vol.%, *P < 5* max. 5 vol.%, *P10* max. 10 vol.%, *P15* max. 15 vol.%, *P10–20* 10–20 vol.%, *P.I.* porphyritic index vol.%, *M* Microphenocryst, *RC* resorbed cryst, *X* Xenocryst, *TR* traces, *F* fall, *Fl* flow, *PyFl* pyroclastic flow, *S* surge, *WS* wavy surge, *PbS* planar bedded surge, *LSU* litho-stratigraphic unit, *Mica* Biotite/phlogopite, *Sanid.** Seymour and Vlassopoulos (1992)

chemistry have been described in numerous contributions (e.g. Davis 1967; Di Paola 1974; Vougioukalakis 1984, 1993; Bohla and Keller 1987; Rehren 1988; Wyers and Barton 1989; Lodise 1987; St. Seymour and Lalonde 1990, St. Seymour and Vlassopoulos 1989, 1992; Ganseki 1991; Limburg and Varekamp 1991; Francalanci et al. 1995; Innocenti et al. 1981; Volentik et al. 2002; Vanderkluysen and Volentik 2002; Buettner et al. 2005; Volentik et al. 2005; Vanderkluysen et al. 2005; Francalanci et al. 2007; Martin 2008; Zellmer and Turner 2007; Longchamp et al. 2011; Bachmann et al. 2011; Spandler et al. 2012; Guillong et al. 2013; Zouzias and Seymour 2014). These papers provide an ever-expanding data set, with which the evolution of the magmas from their generation in the mantle and until their eruption at the surface can be deduced.

The following chapter forms an attempt to compile all available published data (mineralogy, petrography and bulk-chemistry of major and trace elements, and isotope geochemistry) to provide an up-to-date discussion on the magmatic evolution of the volcano in space and time.

A summary of the mineralogy and petrographic characteristics of the units is presented in Table 4.1, based on the studies of Di Paola (1974), Seymour and Vlassopoulos (1989, 1992), Limburg and Varekamp (1991), Francalanci et al. (1995), Wyers and Barton (1989), Vanderkluysen et al. (2005) and own unpublished data and observations. The volcanic products are described according to their litho-stratigraphic succession and regional distribution as it has been done in the previous geological and volcano-tectonic (structural) chapters. Although a large amount of mineralogical observations and bulk-chemical analyses of volcanic and pyroclastic rocks have been published, detailed mineralogical studies are very sparse and partly incomplete.

4.2 Mineralogy and Petrography of the Magmatic Products

This section of the book is meant to give a general overview of the petrographic features recognized in the volcanic products of Nisyros. A detailed petrographic description is given in the Electronic Supplementary Material Appendix of Chap. 4.2 (4.3 ff.).

4.2.1 General Features

A summary of the main mineralogical and petrographic characteristics of the volcanics is given in Table 4.1. A characteristic feature of both mafic and felsic rocks is their highly porphyritic texture, with up to 60 vol.% phenocrysts.

The crystallization sequence, observed in thin section is:

(1) Basaltic andesites to andesites: Plagioclase + clinopyroxene/amphibole + orthopyroxene ± olivine ⟶ plagioclase + clinopyroxene/amphibole + orthopyroxene;
(2) Basaltic andesites to rhyolites: Plagioclase + clinopyroxene/amphibole + orthopyroxene ± olivine ⟶ plagioclase + amphibole + orthopyroxene ± clinopyroxene, apatite, zircon, sanidine, biotite, and quartz.
(3) Dacites and rhyodacites are volcanic rocks derived from differentiated magmas, which underwent magma mixing and mingling processes to various degrees exhibiting antecrysts, xenocrysts, quenched magmatic enclaves and xenoliths. The groundmass consists of rhyolitic residual glasses.

Plagioclase (plg), up to 5 mm in size, shows the highest phenocrysts proportion in all units with up to 70 vol.%, and is mostly zoned (Figs. 4.1 and 4.3), with frequent resorbed cores and often exhibits disequilibrium sieve textures (Fig. 4.2). Its composition ranges from An_{90} in the basaltic andesites to $An_{25–35}$ in the rhyolites. Compositions in basaltic andesites and andesites are: cores $An_{88–55}$, rims: $An_{82–35}$.

Plagioclase crystals in the dacites, rhyodacites, and in some rhyolites have oscillatory zoning (ranging from bytownite to oligoclase) that is sometimes related to disequilibrium textures. Their counterparts from the mafic enclaves are generally reversely zoned. Enclave phenocrysts exhibit rounded cores with distinct rims, normal and superimposed oscillatory zoning;

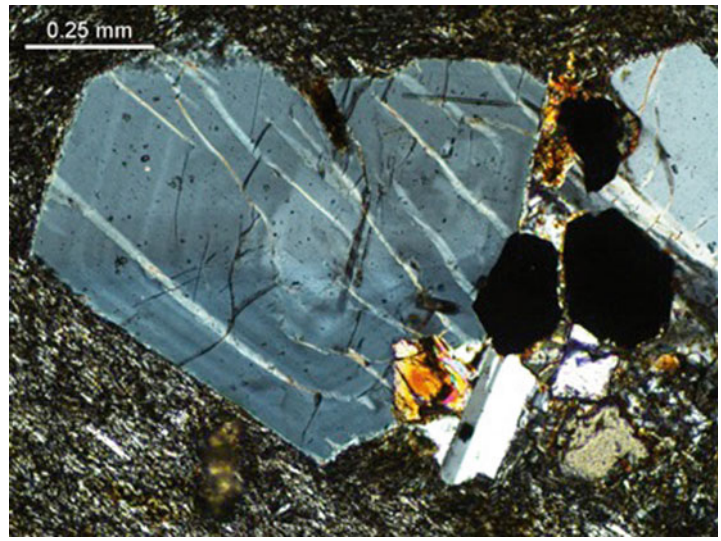

Fig. 4.1 Plagioclase with oscillatory zoning, plagioclase, olivine, and clinopyroxene within a hyalopilitic and fluidal matrix of plagioclase, clinopyroxene and glass. XPL (*crossed polarized light*) image

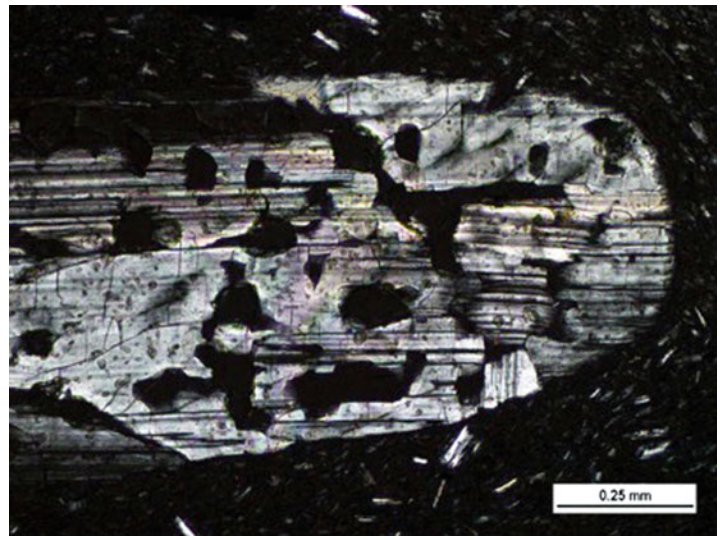

Fig. 4.2 Resorbed twinned plagioclase with sieve textures represented by glass inclusions [PPL, XPL]. Locality: rhyolite (unit No. 17) west of Avlaki Bay

cores $An_{66–33}$ and rims $An_{36–27}$ (Wyers and Barton 1989; Seymour and Vlassopoulos 1992; Braschi et al. 2014; Zouzias and Seymour 2014).

Olivine (ol), slightly zoned, occurs in basaltic andesites and andesites as phenocrysts (Figs. 4.4 and 4.5) and microphenocrysts reaching 0.07 mm in size and ranges from Fo_{82} in basaltic andesites to Fo_{65} in the andesites, partly iddingsitized and rimmed by orthopyroxene. The core composition ranges from $Fo_{82–67}$ whereas the rims are of $Fo_{78–60}$.

Clinopyroxene (cpx) is ubiquitous throughout the series from basaltic andesites to rhyolites, however in various different compositions from augite to ferroaugite, partly reversely zoned. Resorbed pigeonite is also present in some of the rhyolites, but in subordinate amounts. Cpx are frequently rounded and resorbed within the intermediate andesitic, dacitic and rhyodacitic rocks. In the dacites and rhyodacites it is often rimmed by dark, fine-grained opaques reaction assemblages. Reversely zoned pyroxenes are present in enclave-bearing lavas. The following ranges of cpx composition have been reported by Wyers and Barton 1989; St. Seymour and

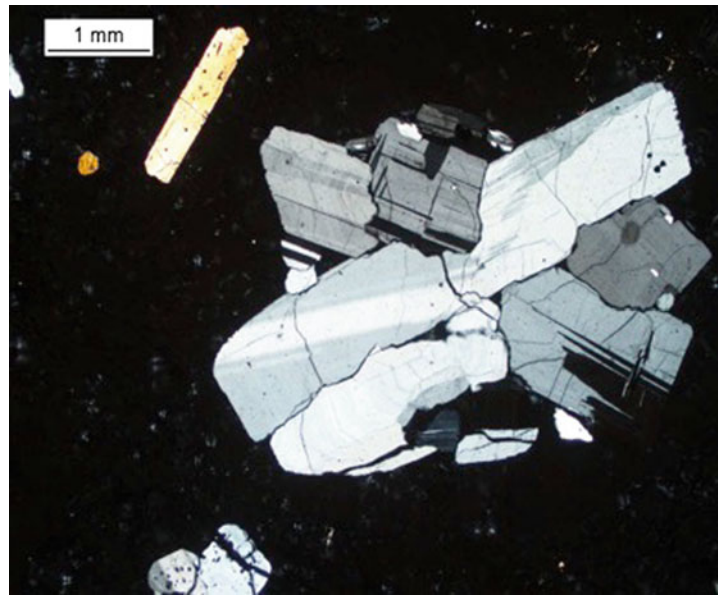

Fig. 4.3 Plagioclase and enstatite in fresh, vesicle-rich glassy matrix from the *upper pumice* (unit No. 32); XPL image

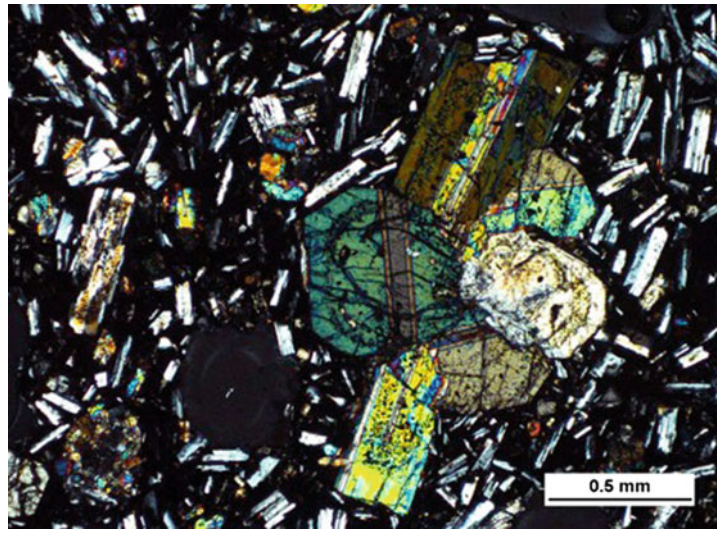

Fig. 4.4 Cross-twins of zoned clinopyroxene and zoned altered plagioclase phenocrysts embedded in a hyalopilitic matrix of pillow lava (unit No. 1); XPL images

Vlassopoulos 1992; Mitropoulos and Tarney 1992; Martin 2008:

- Basaltic andesites cores Mg/(Mg + Fe^{2+}) = 0.814–0.690, rims Mg/(Mg + Fe^{2+}) = 0.836–0.690;
- andesites cores Mg/(Mg + Fe^{2+}) = 0.810–0.702, rims Mg/(Mg + Fe^{2+}) = 0.798–0.694;
- dacites and rhyodacites cores Mg/(Mg + Fe^{2+}) = 0.780–0.691 and rims Mg/(Mg + Fe^{2+}) = 0.734–0.676, and reversely zoned cores Mg/(Mg + Fe^{2+}) = 0.719–0.665.

Magnesium-rich orthopyroxene (opx), enstatite occurs in the andesites and evolves to more *iron-rich compositions* with grain sizes up to 2 mm in the dacites and rhyolites. The compositional ranges of the reversely zoned orthopyroxene in the dacites, rhyodacites and rhyolites are: cores Mg/(Mg + Fe^{2+}) = 0.674–0.580 and rims Mg/

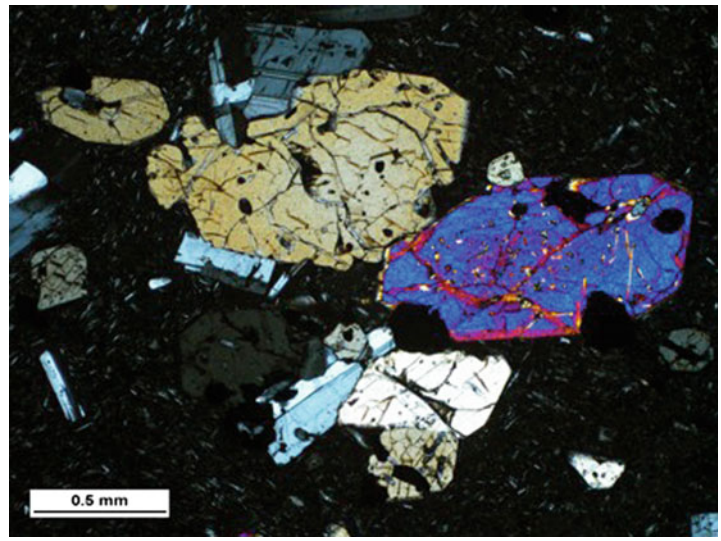

Fig. 4.5 Clinopyroxene clots with interstices filled with glass in dacite (unit No. 25). XPL images

$(Mg + Fe^{2+}) = 0.640–0.590$. Rare occurrences in basaltic andesites and andesites are resorbed antecrysts, partly rimmed by clinopyroxene.

Amphibole (amph) occurs in rhyodacites, rhyolites and dacites as magnesio-hastingsites, sometimes resorbed and often rimmed by opacitic reaction coronas and affected by the oxy-hornblende reaction (thus changing the colors of the crystals and increasing their pleochroism). In addition, kaersutite has been found in dacites (Seymour and Vlassopoulos 1992), pargasite, ferroan-pargasite, magnesium-hornblende and actinolitic-hornblende in gabbro-cumulates and in evolved interstitial melts.

Biotite (bio) phenocrysts have only been found as interstitial phase in some dacites and rhyolites of units 17, 25, 28, 30 (e.g., Electronic Supplementary Material Appendix of Figs. 4.36c and 4.39c).

Sanidine is mostly absent in the evolved dacites to rhyolites. However, Seymour and Vlassopoulos (1989) and Vanderkluysen and Volentik (2002) reported traces as microphenocrysts in dacites, rhyodacites and rhyolites. The rarity of sanidine explains the lack of proper absolute age determinations. Microprobe analyses have shown that potassium is concentrated in the microcrystalline matrix and glass.

Quartz is rare and occurs sporadically as anhedral and partly resorbed crystals in rhyodacites and rhyolites.

Fe–Ti Oxides are rare in basaltic andesites and occur mainly as microphenocrysts. They also occur sporadically in andesites as inclusions in plagioclase, clinopyroxene and olivine. Titanomagnetite (mgt) varies in composition; Al_2O_3 varies from 1.5 to 2.5 wt%, MgO from 0.97 to 1.94 wt%. Ilmenite shows small compositional variations and occurs in dacites, rhyodacites and rhyolites.

Accessory minerals are: Apatite, zircon and various sulfides. Apatite occurs as inclusions in clinopyroxene and in plagioclase. In the evolved lavas it is found as microphenocrysts and within gabbroic clots. Zircon is very rare and occurs in the evolved lavas either within Fe–Ti oxides or as microphenocrysts.

4.2.2 Crystal Clots (Glomerocrysts Syn.)

Crystal-clot minerals (Stewart 1975; Boettcher 1977; Garcia and Jacobson 1979; Girard and Stix 2009; Ellis et al. 2014), synonym to glomerocrysts as polycrystal aggregates occur in many basaltic andesites, andesite, dacite, rhyodacite and rhyolitic lavas of Nisyros and represent primary igneous phase assemblages. According to the theory of (Williams et al. 1954) crystal clots are random accumulations of phenocrysts that may have formed during flowage of a crystal-rich magma. However, they could also originate from

the cumulate layer in a magma reservoir. In the Nisyros lavas, the mineralogy of the crystal clots usually resembles that of the phenocryst phases. For each eruptive unit they display diverse modal proportions. Basaltic andesites and andesites contain clots of ol+plag+mg (Fig. 4.6), cpx+mgt, opx+mgt, cpx+opx+plag+mgt, cpx+plag+mgt, opx+plag+mgt, and plag+mgt (Fig. 4.7), whereas dacites, rhyodacites, and rhyolites show clots of opx+mgt, cpx+opx+plag+mgt, opx+plag+mgt, and amph+plag+mgt+-ilmenite, amp+mgt+-ilm, and plag+mgt. These clots could not have been originated from breakdown reactions of amphibole precursors.

4.2.3 Xenoliths and Enclaves

Properly crystallized and irregular shaped rock inclusions, which were solid prior to the eruption of the magmas, are described as xenoliths, whereas ovoid to irregular shaped inclusions bearing indicators of cooling processes (quench phenomena representing rapid cooling and

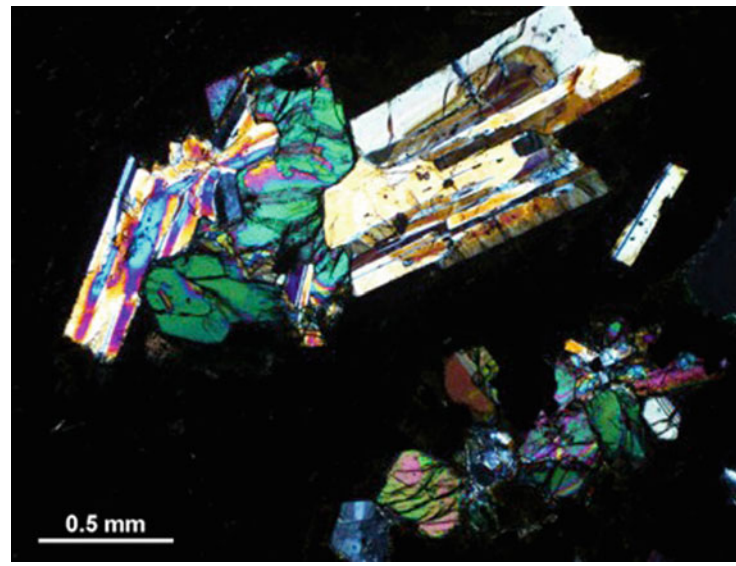

Fig. 4.6 Glassy basaltic andesites lava No. 10 with sparsely porphyritic and vitrophyric texture; plagioclase-olivine-clinopyroxene clots embedded in a hyaline to hyalopilitic glassy matrix. Locality: *middle part* of inner caldera road. XPL image

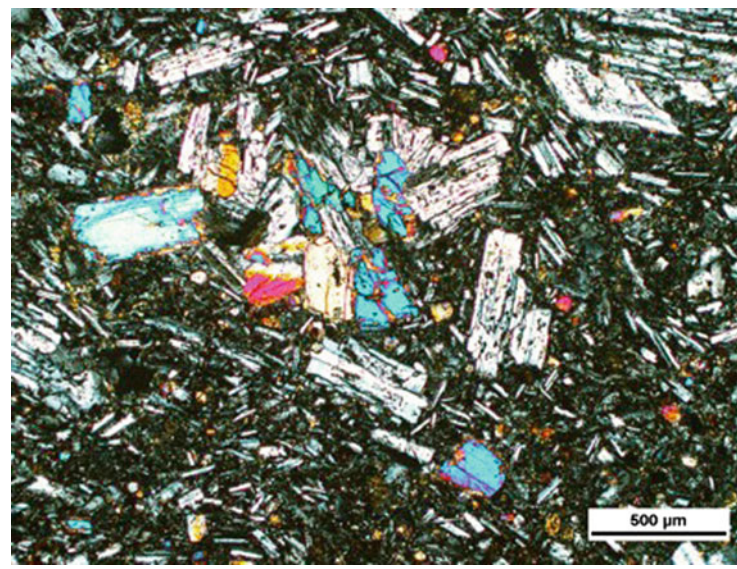

Fig. 4.7 Andesite lava No. 5 with highly porphyritic and glomeroporphyritic textures; plagioclase-clinopyroxene clots embedded in a hyalopilitic matrix of subhedral plagioclase and clinopyroxene micro-phenocrysts and glass. Larger clinopyroxene crystals are rimmed by orthopyroxene. Olivine is rare. Locality: *lower part* of inner caldera road. XPL image

crystallization, quenched rims, vesicular, arborescent, intersertal, hypocrystalline, and hypohyaline textures with interior acicular an skeletal mineral shapes) are designated as enclaves.

Injection of hot basaltic to andesitic melt into a magma reservoir filled with cooler dacitic to rhyolitic melt may cause rapid cooling and quenching leading to rounded and elliptical shapes of enclaves (Eichelberger 1980; Bacon 1986; Dietrich et al. 1988; Dietrich 1989; Feeley and Dungan 1996). Therefore, the enclaves can be regarded as important witnesses with respect to magmatic mixing and mingling processes.

The xenoliths, which occur in the lavas and pyroclastics throughout the entire history of Nisyros Volcano, have been recognized and described already in certain detail by Di Paola (1974), Vougioukalakis (1984), Lodise (1987), Wyers and Barton (1989), Francalanci et al. (1995), Vanderkluysen et al. (2005), Spandler et al. (2012). Di Paola (1974) did not differentiate inclusions into xenoliths and enclaves and grouped them as "hornblende-rich lavas, hornblende-rich cumulates and contact metamorphic rocks". Lodise (1987) distinguished three types of "enclaves" according to their textures in the "Lower and Upper pumice", as well as in the rhyolitic and rhyodacitic lavas: (1) Granular aggregates of crystals in vesicular glass; (2) Hornblende-rich enclaves of variable textures with quenched rims and amphiboles up to several centimetre forming the interior part; (3) Irregular shaped enclaves with quenched rims and interiors less vesicular but variable in texture from hypocrystalline to porphyritic with granular plagioclase and acicular amphibole.

Wyers and Barton (1989) added a genetic distinction for all inclusions designating them only as xenoliths: (1) Cognate xenoliths on the basis of mineral paragenesis in both the host lavas and occurring xenoliths; (2) Amphibole-rich xenoliths; (3) Accidental xenoliths.

4.2.3.1 Rare Mafic Xenoliths (Gabbro-Cumulates and Gabbro-Diorites)

Sub-rounded and rounded mafic xenolithic inclusions with granular and cumulate textures (aggregates) containing plagioclase, clinopyroxene, orthopyroxene, minor olivine, hastingsitic amphibole and titanomagnetite have been observed in the pyroclastic deposits of the "Lower and Upper pumice". These pyroxenitic, anorthositic, gabbroic and dioritic xenoliths and blocks vary in sizes on a millimeter to several decimeter scale. One large example of a gabbro cumulate is shown in Figs. 4.8a, b and 4.9a–f, one example of dioritic xenolith in Figs. 4.10a, b and 4.11a–c.

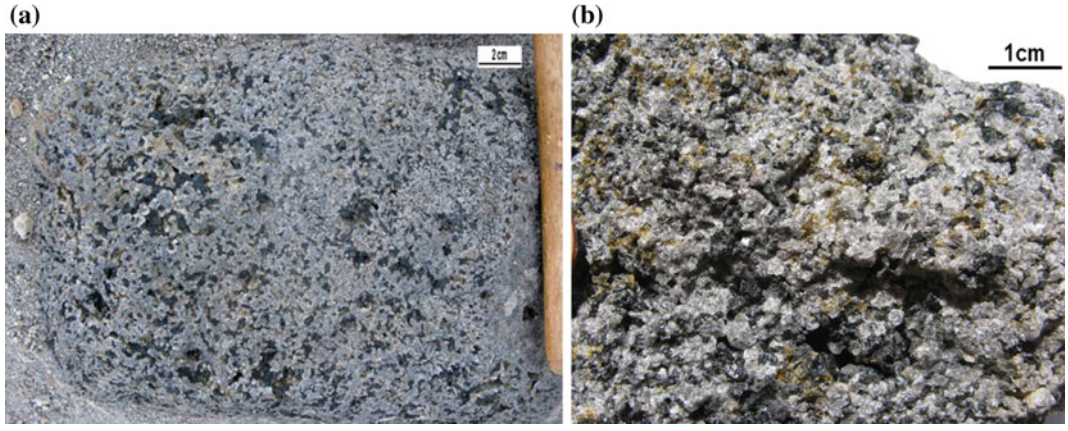

Fig. 4.8 **a** Gabbroic cumulate block (~20 × 30 cm) found in "*lower pumice*" (unit No. 28); grey crystals: plagioclase; *dark-green* and *black* crystals: clinopyroxene and amphibole; *yellowish-green* crystals: olivine. **b** Fresh, broken hand-specimen showing the cumulate and granular texture with crystals up to a few millimetre in size (Fig. 4.9a–f). The interstitial microcrystalline and porous dacitic matrix is partly broken out

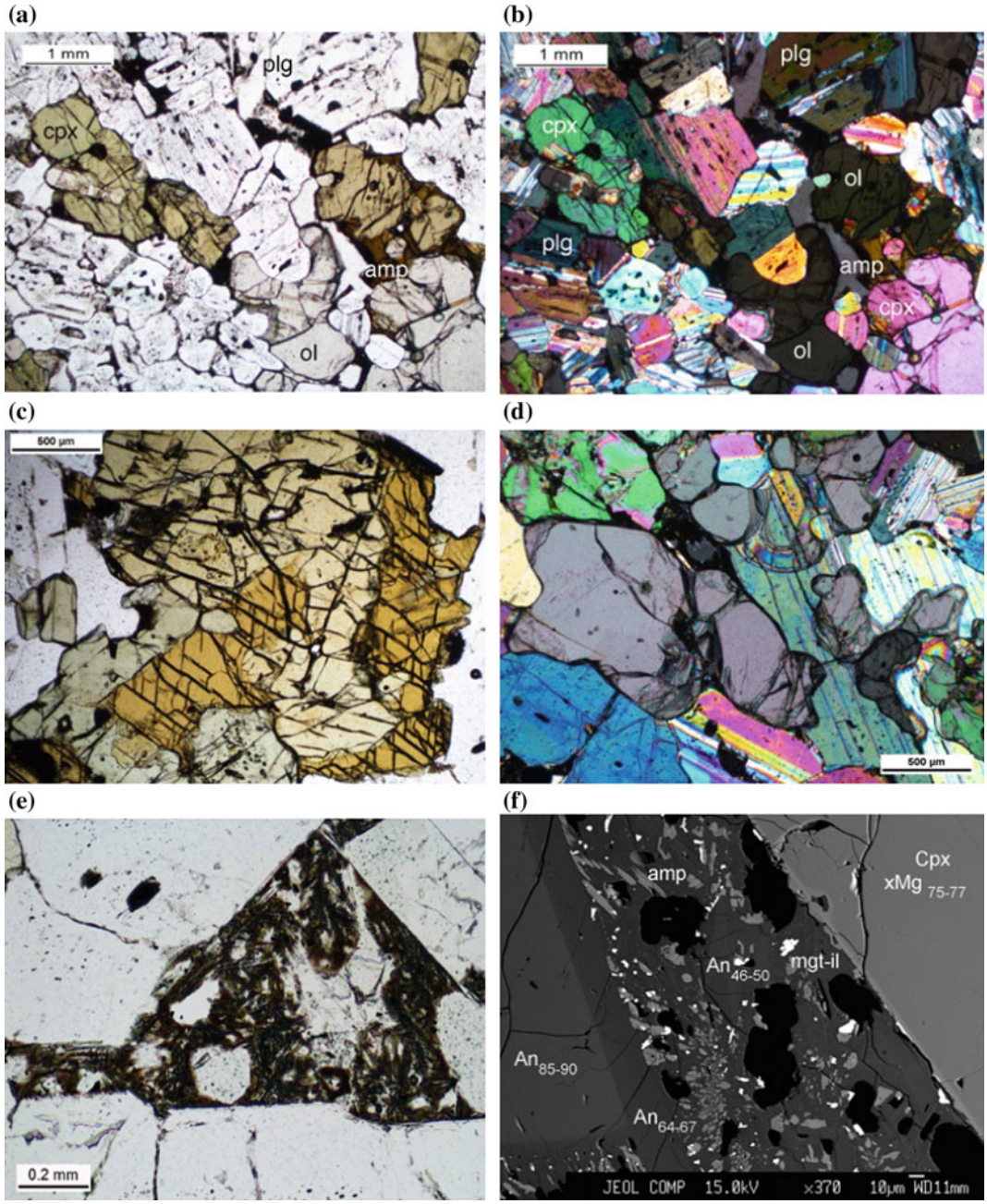

Fig. 4.9 **a** and **b** Gabbroic cumulate with well-equilibrated adcumulate texture of plagioclase (*plg*), clinopyroxene (*cpx*), olivine (*ol*), and amphibole (*amp*) as rims around clinopyroxene and interstitial microcrystalline quenched basaltic matrix. Plagioclase is sieved with fine melt inclusions. (**a** *PPL* plan polarized light and **b** *XPL* cross polarized light). **c** Intergrowth of magnesio-hastingsitic amphibole (*x*Mg = 0.79 and small pargasitic rims with *x*Mg = 0.74); augitic clinopyroxene (*x*Mg = 0.75–0.77) in gabbroic cumulate; (PPL). **d** Intergrowth of olivine (*x*Mg = 0.77) with (**c**) clinopyroxene and twinned plagioclase in gabbroic cumulate (XPL, $An_{85–90}$, rimmed with $An_{64–67}$). **e** Close-up of interstitial microcrystalline quenched basaltic matrix between plagioclase crystals consisting of plagioclase microliths and quenched glass of andesitic to dacitic composition (**e** PPL). **f** Backscatter image of the interstitial matrix with relicts of quenched glass, intermediate plagioclase ($An_{64–67}$ and $An_{45–50}$), ferroan-pargasite, magnesio-hornblende, actinolitic-hornblende and magnetite-ilmenite. *PPL* plane polarized light, *XPL* crossed polarized light

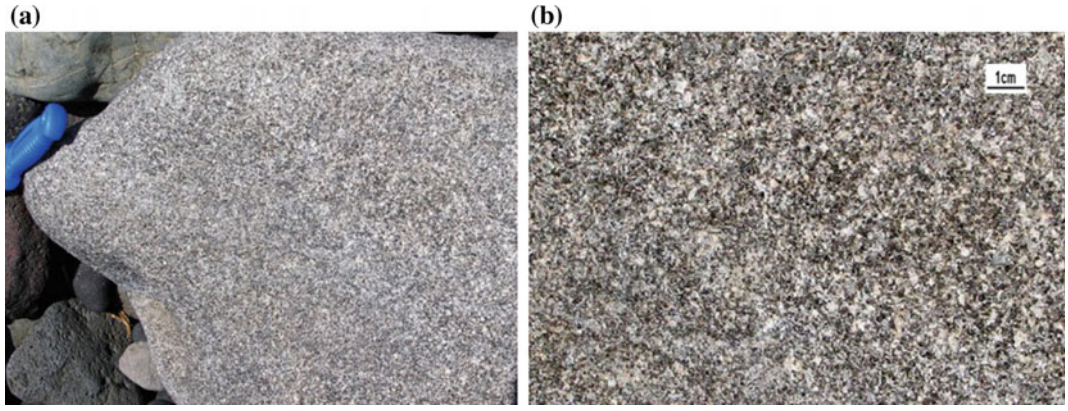

Fig. 4.10 **a** Fine-grained gabbro-dioritic block (~30 × 40 cm) with weathered surface found in rhyolitic pyroclastics (unit No. 28, lower pumice); *grey* crystals: plagioclase; *dark-green* and *black* crystals: clinopyroxene and amphibole. **b** Fresh, broken hand-specimen showing the granular texture with crystals up to a few millimeter size

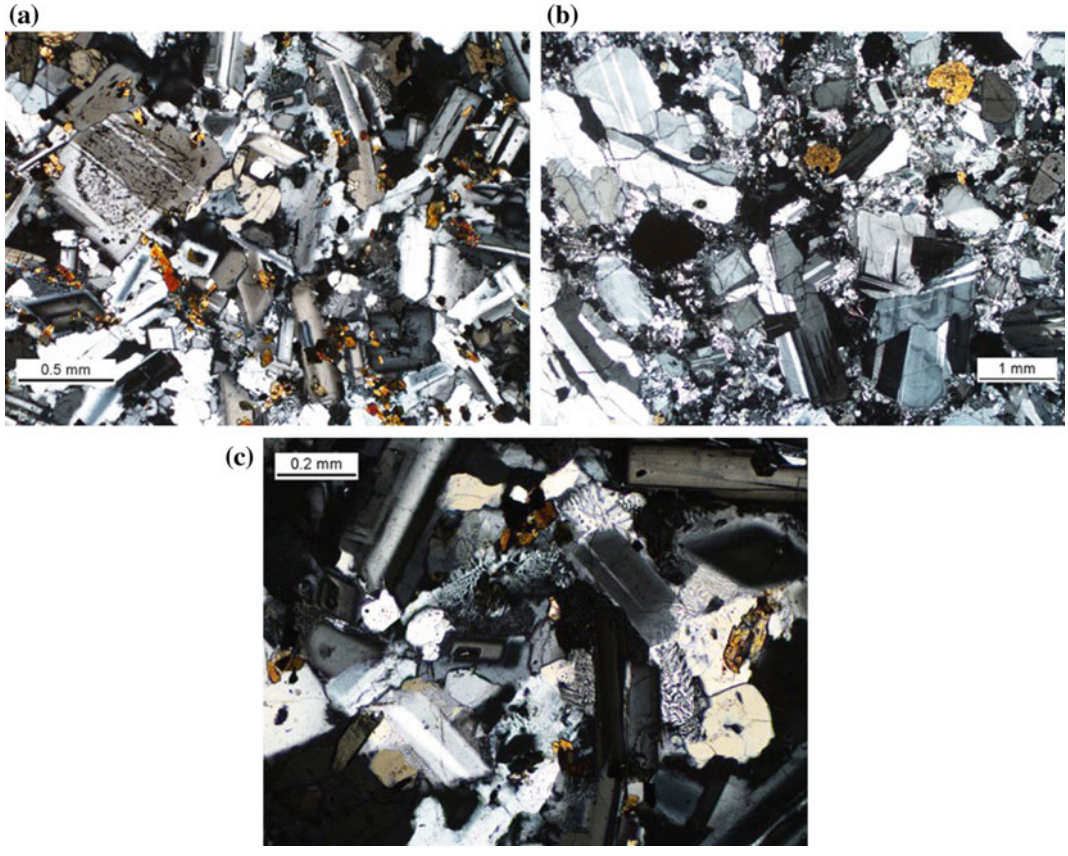

Fig. 4.11 **a–c** Weakly porphyritic micro-diorite (xenolith from lower pumice No. 28) with intergranular texture of plagioclase. Plagioclase phenocrysts are zoned with higher anorthitic cores and sieve texture. The interstices are occupied by small grains of euhedral green amphibole, minor clinopyroxene, and opaques. In addition, many interstices are filled with myrmekite patches (quartz worms penetrating plagioclase **b** and **c**). All images XPL

4.2.3.2 Quenched Mafic Enclaves

The abundance of enclaves increases in time and space: enclaves are very rare in the early volcanic cycles. No dacitic magmas have been formed during this period. During the composite strato-volcano cycles, dacites (Unit No. 14) were extruded within the central part of an early Nisyros volcanic environment and contained up to 30% andesitic enclaves (Figs. 4.12 and 4.13). However, they differ from enclaves in the younger rocks due to the absence of amphibole. Amphibole-bearing enclaves appears in the younger dacites in the lavas and pyroclastics of Afionas and Lies tuff cones (Units No. 18 and 19) and in the rhyolitic lava domes and flows of Stavros and Avlaki (Unit No 17). Up to 2% andesitic enclaves carrying minor amounts of amphibole are included in the voluminous dacitic lavas of Emborios (Unit No. 25). Lodise (1987) and Gansecki (1991) described a steady increase of enclave frequency from the lower pumice (Unit No. 28) throughout the lava flows of Nikia

Fig. 4.13 Dacite from lava (No. 14), rich in *grey* and *reddish* enclaves that make up to 30 vol. %

Fig. 4.12 Polished block of enclave-rich dacitic lava (No. 14), which is dominated by reddish, oxidised enclaves in a black glass-rich matrix, the latter appearing to be less than 10 vol.%. Under the microscope the components seem to be only agglutinated and not welded

Fig. 4.14 Quenched enclaves of andesitic composition from the Drakospilia lava flow (Unit No. 32) in the southwest of Nisyros volcano. *Photo* Barry's Ramblings

(unit No. 30) and the upper pumice deposits (unit No. 31) to the post-caldera rhyodacite domes (unit No. 32) (Fig. 4.14).

The enclaves found in the post-caldera lavas are dominated by intergrowths of acicular amphiboles and plagioclase crystals, have vesicular textures and can vary on a centimetre to decimetre scale (Fig. 4.15). They usually show quenching textures. These lavas also contain numerous millimetre-sized round and oval xenolithic undeformed inclusions with hypocrystalline, intergranular, and intersertal textures, which do not exhibit quench textures but resemble small fragments of pre-existing hypabyssal lavas.

4.2.4 Amphiboles as Phenocrysts and Resorbed Xenocrysts

Amphiboles are common mafic minerals in the volcanic rocks of Nisyros Island. They occur in dacitic, rhyodacitic and rhyolitic lavas and pyroclastics, but are less frequent in andesites and only as relics in basaltic andesites. Depending on the magmatic environment, the amphiboles show a large variation in mineral chemistry from magnesio-hastingsite (close to pargasitic transition) through evolved hastingsite to hornblende (Table 4.2). Tschermakitic hornblende and kaersutite have been found in dacites and rhyodacites with relatively high TiO_2 between 3.2 and 4.2 wt % and K_2O between 0.34 and 0.7 wt% (Wyers and Barton 1989; Seymour and Vlassopoulos 1992). The amphiboles in rhyolites display greenish to light brownish pleochroic colours and euhedral shapes (Fig. 4.16) and are mainly of magnesio-hastingsite composition with lower TiO_2 values between 2.1 and 2.8 wt%. However, in most cases the amphiboles are partly resorbed and also show black, opacitic rims of variable thickness (Figs. 4.17, 4.18 and 4.19). There is clear evidence that the amphiboles decomposed to crystallize clinopyroxene, orthopyroxene, titanomagnetite and ilmenite and to release water (Figs. 4.17, 4.18 and 4.19; Table 4.3).

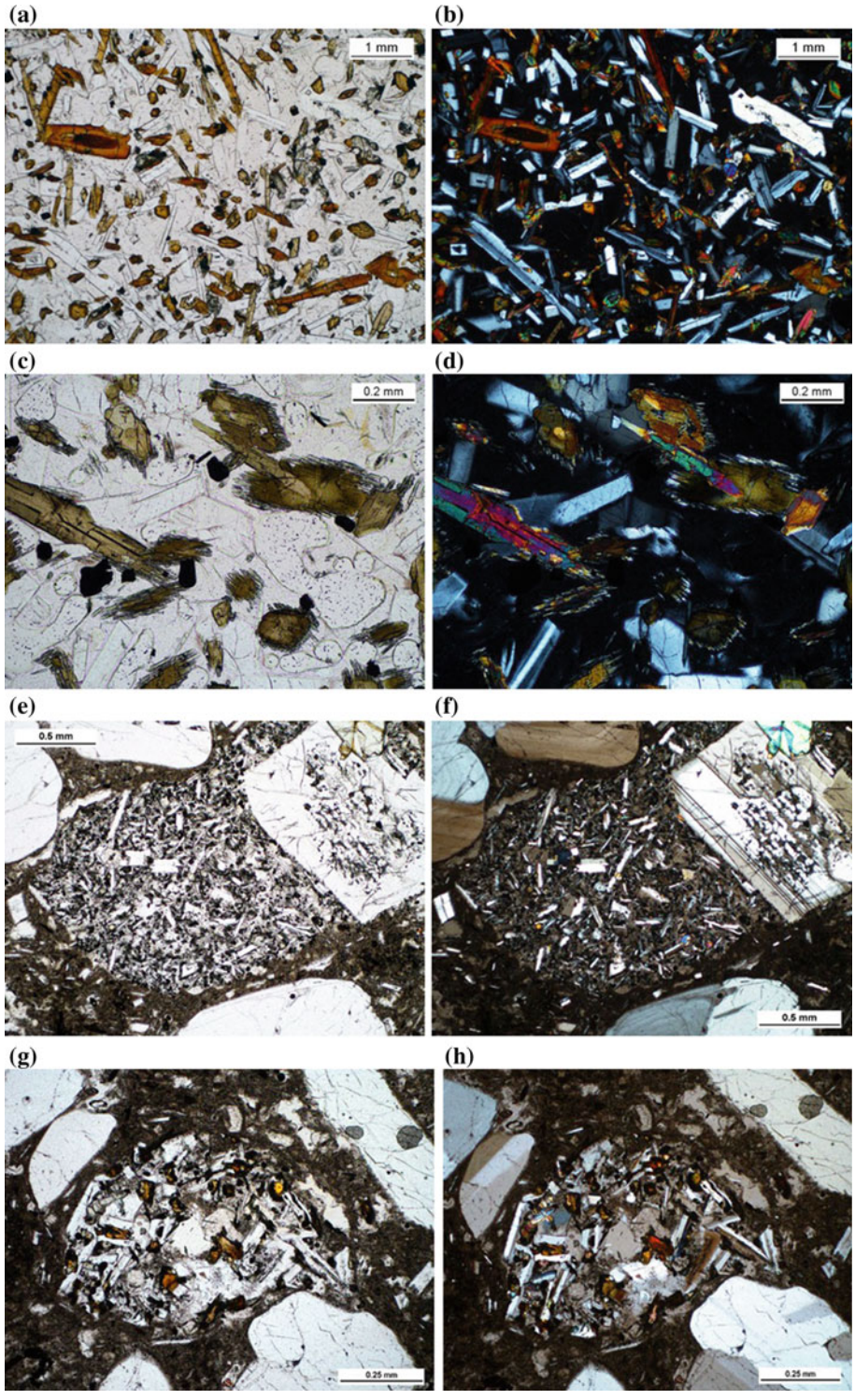
(a)
1 mm
(b)
1 mm
(c)
0.2 mm
(d)
0.2 mm
(e)
0.5 mm
(f)
0.5 mm
(g)
0.25 mm
(h)
0.25 mm

◀ **Fig. 4.15** **a**, **b** Detail of weakly vesicular enclave with intersertal texture, consisting of plagioclase and *red brown* acicular hastingsitic amphibole. Larger euhedral plagioclase is zoned. Clinopyroxene is subordinate. Titanomagnetite is accessory. **c**, **d** Vesicular enclaves are dominated by up to several millimetre size acicular *brownish-green* amphiboles intergrown with plagioclase. The amphiboles show reaction coronas of *light green* orthopyroxene. Clinopyroxene and small euhedral shaped titanomagnetite is accessory. The interstitial groundmass with hypohyaline texture consists of plagioclase, partly devitrified glass and numerous small round vesicles. **e**, **f** Small (<0.5 mm) round xenolithic inclusion mainly consisting of plagioclase and minor amphibole and orthopyroxene. **g**, **h** Very small (<0.25 mm) round xenolithic inclusion, mainly consisting of two generations of plagioclase and minor amounts of orthopyroxene and Fe–Ti oxides

The euhedral amphiboles within the magmatic enclaves are magnesio-hastingsites (Figs. 4.5a, b) with higher Al, Ti, Ni and Na but lower Mn contents than the amphiboles in the rhyodacites. They display strong brownish to red brownish pleochroic colours. They are often normally zoned with Fe-enrichment towards the rims. The magnesio-hastingsites, pargasites, and ferroan pargasites, found in the gabbro cumulate (Fig. 4.5) have compositional ranges, which are shown in Table 4.2.

4.2.5 Amphibole Breakdown Reactions Rims

Amphibole reaction rims are common phenomena in andesites, dacites and rhyolites of arc magmas and display a broad range of textures and mineralogy. A first classification was given by Garcia and Jacobson (1979), later by Rutherford and Hill (1993); a comprehensive review combining experimental studies by De Angelis et al. (2015). In the South Aegean

Table 4.2 Amphibole compositions in the gabbro-cumulate xenolith found in the "lower pumice" (Unit No. 28) of Nisyros Volcano

wt%	Magnesio-hastingsite	Pargasite	Ferroan pargasite	Magnesio hornblende	Actinolitic hornblende
SiO_2	42.0–42.4	41.9–42.2	41.6	45.7–48.5	51.9
TiO_2	3.2–3.5	3.1–3.5	2.35	1.9–2.41	1.51
Al_2O3	12.5–12.7	12.5–12.8	12.3	6.5–7.1	12.53
Cr_2O3	0.05–0.10	0.05–0.12	0.02	<0.01	<0.01
Fe_2O_3	2.7–3.1	0.1–0.4	0.75	n.d.	n.d.
FeO	6.9–7.3	9.2–9.5	13.18	10.4–12.3	9.6
MnO	0.07–0.15	0.09–0.13	0.24	0.27–0.34	0.3
NiO	0.0–0.01	0.01–0.05	0.01	0.0–0.2	0.02
MgO	15.0–15.2	15.1–15.3	13.7	12.7–13.15	8.54
CaO	11.5–11.7	11.6–11.7	9.85	17.5–17.65	10.49
Na_20	2.54–2.70	2.54–2.65	2.62	0.56–1.05	3.56
K_20	0.31–0.33	0.31–0.33	0.38	0.01–0.03	0.53
H_2O	2.06–2.07	2.06–2.07	2.01	2.04–2.09	2.14

Ad-cumulate amphiboles are of magnesio-hastingsite, pargasite and ferroan pargasite composition, whereas magnesio-hornblende and actinolitic-hornblende are found in the interstices. The amphibole compositions, using the nomenclature of Leake (1978) and Leake et al. (1997), were normalised by assuming (i) fixed $Fe^{3+}/(Fe^{3+} + Fe^{2+})$ ratio of 0.2 and 23 oxygens, and (ii) cations—Ca–Na–K = 13, as well as the program of Spear and Kimball (1984) estimating Fe^{3+} based on stoichiometric constraints of the total amphibole crystal chemistry

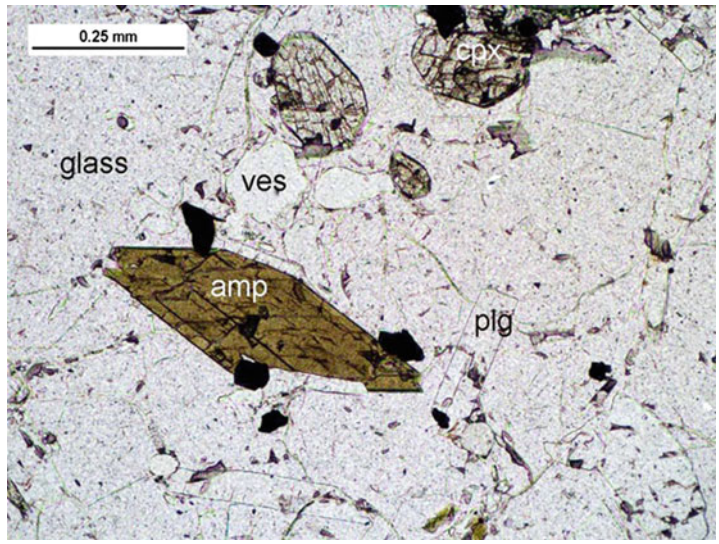

Fig. 4.16 Euhedral shaped hastingsitic amphibole with thin opacitic black rims, sodic plagioclase and clinopyroxene in the glassy part of the Nikia rhyolitic lava (No. 30); opaque crystals are Ti-magnetite and ilmenite; vesicles (*ves*) are partly filled with fluid inclusions; PPL image

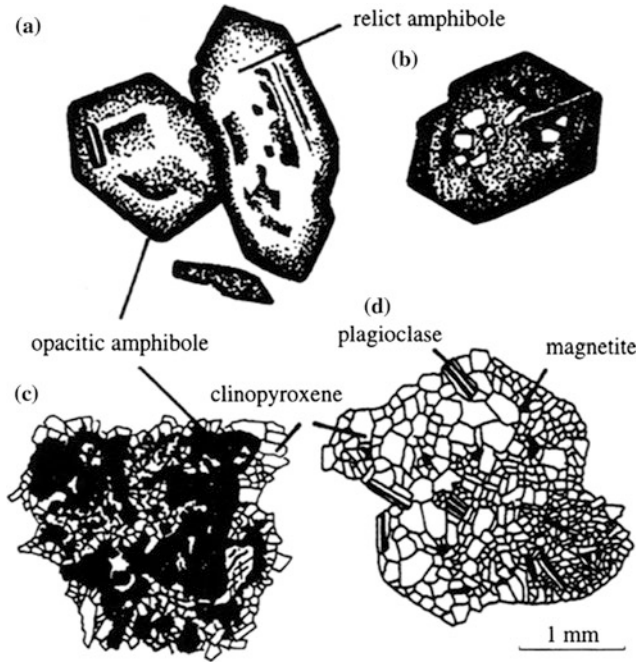

Fig. 4.17 **a** The *black-rimmed* phenocryst type of amphiboles with euhedral to anhedral and rounded shapes and very fine black and dusty aggregate rims of iron oxides (e.g. ilmenite) and small pyroxene crystals. **b** The *black rim* growth proceeds inward from the crystal margin. **c**, **d** show the "gabbroic type" reaction, which is caused by the breakdown reaction of the amphibole and leads to crystal growth of coarser clinopyroxene-plagioclase-magnetite aggregates. The opacite aggregate sometimes contains relicts of amphibole, preserving its original composition. The figure is taken from Dietrich et al. (1988)

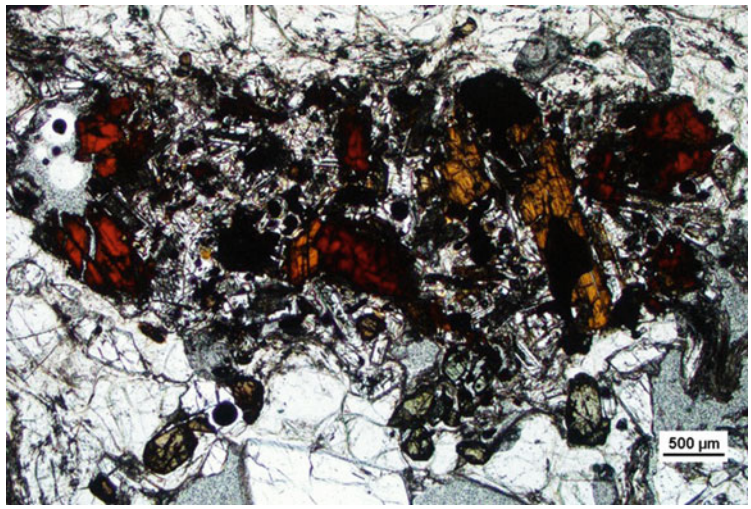

Fig. 4.18 Typical disintegrated amphibole, plagioclase, ortho- and pyroxene, Fe–Ti oxide assemblage in a glassy, vesicle-rich rhyolitic lava (Unit No. 30). The amphibole relics have *reddish pleochroitic colours*, due to oxy-hornblende reactions; image under PPL

Volcanic Arc amphibole breakdown reaction rims have been described in detail by Dietrich et al. (1988) and Gartzos et al. (1999) (Figs. 4.17a–d). In contrast to crystal clots, crystal reaction rims form microliths to equigranular assemblages (syn. corona) of opx +cpx+Fe–Ti oxide ± plagioclase that occur around relict amphibole. The amphiboles in the Nisyros lavas and pyroclastics are in the majority of cases of hastingsitic composition and show all steps of breakdown reactions (Figs. 4.3 and 4.4).

According to Garcia and Jacobson (1979) two distinct types of amphibole reaction products occur in the evolved lavas and formed as a result of dehydration:

(1) The majority of amphiboles occur as the "black-rimmed type". Some of the amphibole is partly or entirely replaced by a very fine black and dusty aggregate of iron oxides (e.g. ilmenite) and small pyroxene crystals (Fig. 4.17a, b as well as in Fig. 4.19a–c, g, h). In several cases, the reaction coronas consist of orthopyroxene, clinopyroxene, plagioclase, and Fe–Ti oxide aggregates (Fig. 4.19d, e). The assemblage in the reaction rims is identical with the phenocryst assemblage of the host lava. Besides the rim reaction, the amphiboles sometimes display evidence of the oxy-hornblende reaction (Graham et al. 1984), due to a rise of temperature: the OH bonds are broken and the crystal turns into reddish-brownish colours with intense pleochroism (Fig. 4.19a–c). As heat grades up, other bonds are also broken, the crystal resorbs and other anhydrous minerals start to crystallize.

Fig. 4.19 **a**, **b** Various steps of amphibole breakdown reactions in the rhyolite lava west of Avlaki (Unit No. 17) and Nikia rhyolite (unit No. 30). **a** Isolated euhedral magnesio-hastingsite, slightly rounded with very thin black rim adjacent to anorthitic plagioclase; **b**, **c** up to 40 µm *thick black* rims, formed out of submicroscopic aggregates of Fe–Ti oxides and orthopyroxene; **c** amphibole partly pseudomorph as a micro-granular aggregate of pyroxene and plagioclase; **d** amphiboles with a well developed corona of orthopyroxene needles; **e**, **f** amphibole disintegrated into a granular aggregate of pyroxene, plagioclase and Fe–Ti oxides within a vesicle-rich glassy matrix (**e** in dacite flow unit No. 25 and f in rhyolite flow unit No. 30); **g**, **h** small amphibole grains totally transformed into *black* aggregates of Fe–Ti oxides and pyroxenes. All images in PPL ▶

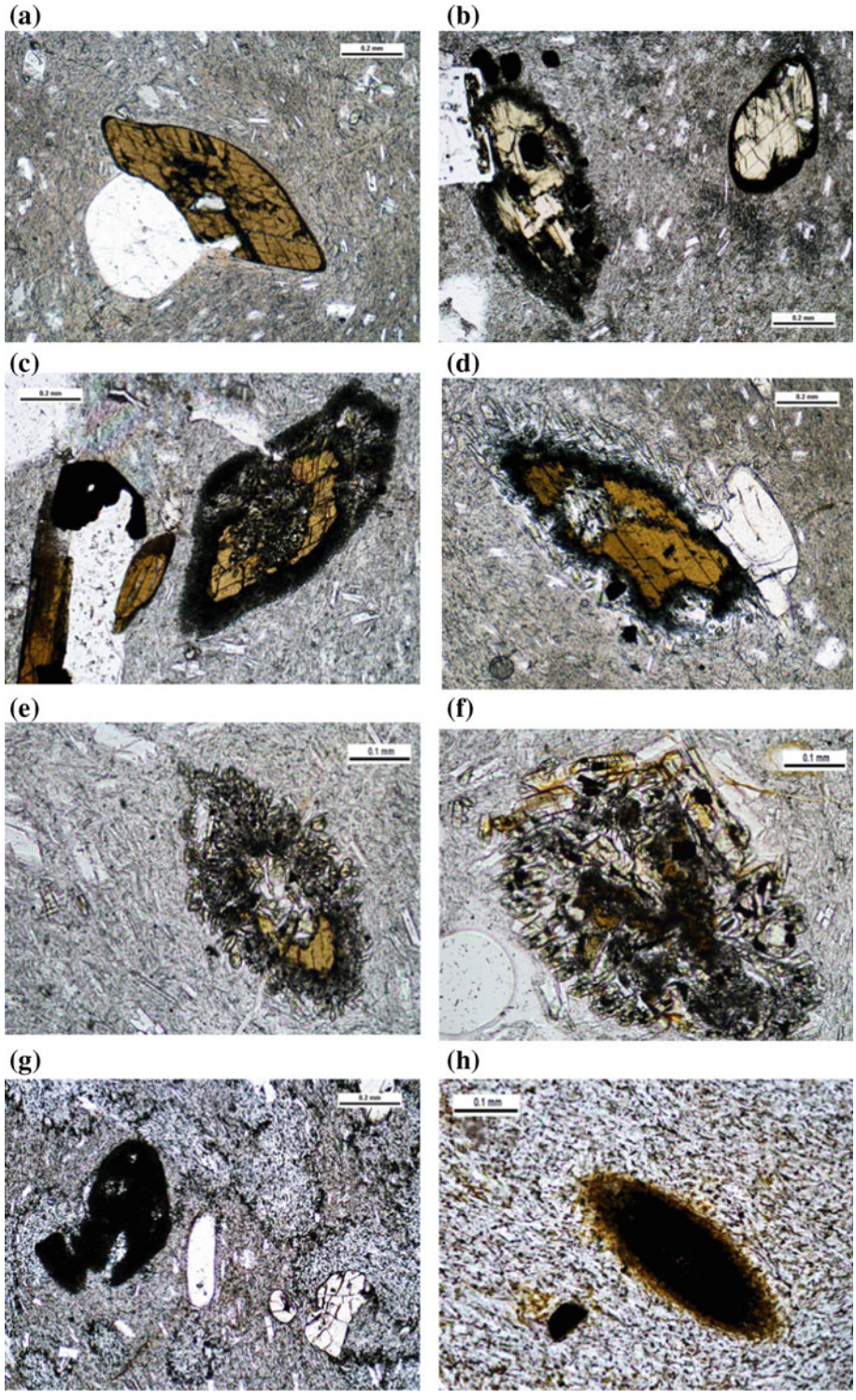
(a)
(b)
(c)
(d)
(e)
(f)
(g)
(h)

Table 4.3 Representative amphibole compositions in the evolved lavas (Units No. 25, 30 and 32) and their mafic enclaves of Nisyros volcano

Mineral	Kaersutite	Mg-hasting	Mg-hasting	Mg-hasting	Mg-hasting	Tscherm.Ho.	Mg-hasting
wt%							
SiO_2	37.8	40.31	41.37	41.51	41.82	43.01	42.75
TiO_2	4.56	2.32	2.12	2.79	2.48	3.2	2.16
AI_2o_3	14.19	12.99	13.32	12.72	13.06	10.88	12.52
FeO(t)	17.8	15.35	11.3	14.45	13.6	13.62	10
MnO	0.28	0.17	0.13	0	0.19	0.17	0.12
MgO	14.75	15.3	15.51	12.48	12.93	12.87	16.21
CaO	0.05	10.84	10.84	11.05	11.7	11.3	11.38
Na_2O	0.56	2.5	2.56	2.47	2.62	2.11	2.33
K_2O	8.14	0.43	0.36	0.34	0.34	0.52	0.38
Total	98.13	100.21	97.51	97.81	98.74	97.68	97.85
Unit	25	30	30	30	30	32	32
Rock	Dacite		Rhyolite		Mat. enclave	Rhyodacite	Maf. enclave

Data from Wyers and Barton (1989) and Seymour and Vlassopoulos (1992)

(2) The rare amphibole type is the so-called "gabbroic type" (Garcia and Jacobson 1979; Rutherford and Hill 1993), which has been observed in the evolved lavas, in the basaltic andesite and andesites. The amphibole is partially replaced by a fine-grained granular aggregate of anhedral ortho- and clinopyroxene, plagioclase and Fe–Ti oxide with mosaic textures (Figs. 4.17c, d and 4.19d–f). In the fine-grained equigranular gabbroic glomerophyres, plagioclase never shows oscillatory zoning.

Both amphibole reaction products, "black-rimmed" and the "gabbroic type" occur in the same lava units. Also minor opacitic relics of amphibole can be recognised in the cores of well-shaped pseudomorph aggregates of clinopyroxene, plagioclase and oxides. These breakdown reaction products may lead to continuous crystal growth of pyroxenes and plagioclase to produce random types of aggregates (Fig. 4.18) and not typical glomeroporphyritic clots.

Often, the euhedral shaped, black-rimmed amphiboles embedded in pumice show no other stages of resorption and dusty effects.

4.3 Whole-Rock Major and Trace Element Geochemistry

A collection of 250 analyses from rock samples with known localities published by Rehren (1988), Seymour and Vlassopoulos (1992), Francalanci et al. (1995), Vanderkluysen et al. (2005), Zellmer and Turner (2007) and Spandler et al. (2012) has been compiled. Whole rocks were analysed for major and trace elements mainly by XRF (i.e. Nb, Zr, Y, Sr, Rb, Pb, Ga, Zn, Cu, Ni, Cr, V, and Ba), whereas Th, Hf and rare earth elements by neutron activation and laser ablation inductively-coupled plasma mass spectrometry (LA-ICP-MS). The values are given in Electronic Supplementary Material Appendix A.

An overview of this data is given in Table 4.4, according to the lithostratigraphic units, rock types and silica contents (SiO_2 wt%).

The chemical trend of all Nisyros volcanics is typical for low to medium potassic calc-alkaline rocks (Fig. 4.20). According to the TAS diagram, the volcanic products of Nisyros fall in the basaltic andesites, andesites, dacites, rhyodacites and rhyolites fields. Since the bulk chemical

Table 4.4 Overview correlation between lithostratigraphic units, lava flows with their enclaves, domes, pyroclastics, rock types and silica contents (SiO_2 wt%)

LSU	Eruption mode	Thickness	Rocktype	Bulk rock	Enclaves	SiO2 wt.%	87Sr/86Sr	LSU
				SiO2 wt.%	SiO2 wt.%	52 54 56 58 60 62 64 66 68 70 72 74		
	Post-Caldera Eruptive Cycle							
33	Lava domes, flows	max. 600 m	Rhyodacite	67.0 - 71.3	54 - 57*		0.70379-0.70462	33
	Caldera Eruptive Cycles and Caldera Collapse							
31	Fl-WS-Fl-PbS-succ.	outcrop 30 m	Rhyolite	67.2 - 72.8	56 - 60*		0.70456	31
30	Lava flows	max. 150 m	Rhyolite	68.5 - 71.8	53 - 56*		0.70419-0.70454	30
28	F-Fl-WS-Fl-succ.	outcrop 20 m	Rhyolite	68.5 - 73.7	57 - 61*		0.70424	28
27	Lava flow	max. 10 m	Andesite	58.9 - 59.5				27
	Composite Stratovolcano Cycles							
26	Dome collapse breccia.	outcrop 20-30m	Dacite	65.0 - 67.0				26
25	Flows	max. 150 m	Dacite	65.0 - 68.7*	58.3 - 60.6		0.70402-0.70462	25
24	Flows	max. 25 m	Bas. And.- And.	53.0 - 59.0			0.70426-0.70465	24
22	Flows	max. 10 m	Bas. And.- And.	54.0 - 59.5			0.70413-0.70459	22
21	F-PbS-PyFl-succ	outcrop 15 m	Bas. And.- And.	54.2 - 58.8			0.70499	21
19	F-S-F-3S-F-F-xS-F-succ.	outcrop 50 m	Bas. And.to Dac.	54.3 - 60.7		?	0.70477-0.70521	
19	F-PbS-Fl-succ.	outcrop 40 m	Dacite	63.4 - 67.6				19
18	Lava flow	? max. 10 m	Dacite	63.5 - 64.8*				18
17	Lava domes, flows	max. 60 m	Rhyolite	69.4 - 73.2*			0.70415-0.70427	17
16	S-Fl-succession	outcrop 30 m	Bas. Andes.	50.8 - 52.0				16
15	Lava flow	max. 40 m	Andesite	58.5 - 59.7			0.70338-0.70466	15
14	Lava flow	max. 25 m	Dacite	65.7 - 67.0	57.8 - 58.5			14
13	Lava flow	max. 40 m	Bas.And.- And.	54.0 - 59.7				13
	Early Shield Volcanic Cycles							
11	F-Fl-F-S-Fl-succ.	outcrop 35 m	Bas.And.- And.	53.7 -56.7				11
10	Lava flows	max. 70 m	Bas. Andes.	54.3 - 55.7				10
8	Lava flow	max. 5 m	Bas. Andes.	53.7 - 56.7				8
6	S-F-Fl-S-Fl-succ.	outcrop 60 m	Bas. Andes.	51.7			0.70354-0.70463	6
5	Lava flows	max. 40 m	Andesite	55.7 - 60.0				5
4	F-Fl-S-F-succ.	outcrop 30 m	Andesite	55.9 - 57.8				4
3	Lava flow	max. 35 m	Bas. Andes.	53.3				3
	Submarine Volcanic Base							
1,2	Pillow & lava flows	? max. 50 m	Bas. Andes.	52.6 - 56.9*			0.70377-0.70452	1,2
						52 54 56 58 60 62 64 66 68 70 72 74		

F fall, *Fl* flow, *S* surge, *PbS* planar bedded surge, *WS* wavy surge, *PyFl* pyroclastic flow, *Encl* enclaves, $^{87}Sr/^{86}Sr$ data from: Francalanci et al. (1995), Gülen (1987, 1990)

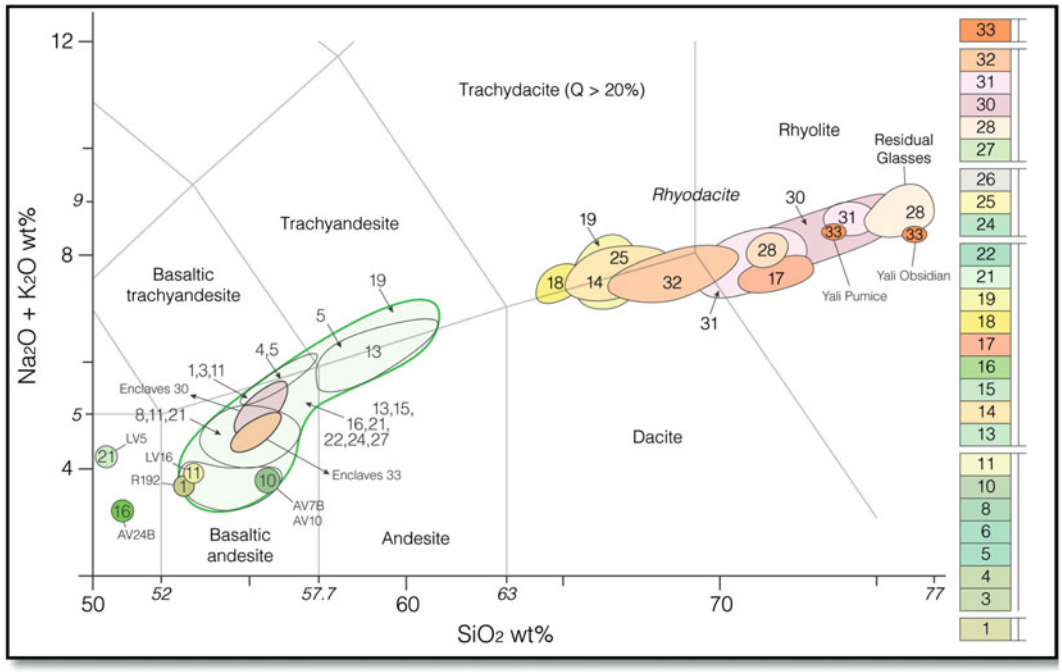

Fig. 4.20 TAS diagram for Nisyros volcanics. The point distribution of the analyzed rocks has been converted into approximate overlapping fields. *Numbers* and *colors* refer to the lithostratigraphic units given in the geological map and lithostratigraphic profiles: from the oldest (*1*) to the youngest (*33*) eruptive unit

composition of these rocks covers a wide range, we describe them in the lithostratigraphic order.

4.3.1 General Geochemical Characteristics

The general differentiation trends of major and selected trace elements of Nisyros volcano are shown in Figs. 4.21, 4.22, 4.23 and 4.24 and overlap with those reported from all volcanic rock series in the Aegean volcanic island arc. They are characterized by an increase of SiO_2, K_2O, Na_2O, Rb, Ba, Ce, La, Zr, Nb and a decrease of MgO, CaO, FeO_{tot}, Al_2O_3, Cr and Ni, which fits the general calc-alkaline trend, marked CA with down-bending arrows in Fig. 4.5. Using the FeO_{tot}/MgO versus SiO_2 diagram of Miyashiro (1974), several basaltic andesites and andesites of the early caldera cycles straddle the arc tholeiitic to calc-alkaline separation line with no apparent compositional gap in the differentiation series (Fig. 4.21). This is also expressed in two compositional trends for basaltic andesites and andesites that allow a division into several differentiated groups, i.e. a normal calc-alkaline trend and a tholeiitic trend towards higher TiO_2 (Tables 4.5 and 4.6; Fig. 4.21). In a few cases, the analyses with high Al_2O_3 contents reveal peraluminous characteristics (Fig. 4.21), which might be an effect of high modal abundances of plagioclase in the samples.

Fig. 4.21 Bulk rock composition of Nisyros volcanics: major oxides plotted against SiO_2 and MgO. **a** The FeO_{tot}/MgO versus SiO_2 diagram (Miyashiro 1974) shows an arc tholeiitic affinity (TH) of several basaltic andesites and andesites of the early caldera cycles, which is also apparent in the TiO_2/MgO and $TiO_2/FeO_{(tot)}$. **c**, **d**: the calc-alkaline trend is marked CA with down-bending arrows in plots (**a**), (**d**), (**e**) and (**h**). In a few cases, the analyses with high Al_2O_3 contents (**e**) reveal peraluminous characteristics. Note the compositional gap in plots (**a**) and (**b**) between andesites and dacites, e.g. already recognized by Wyers and Barton (1989) ►

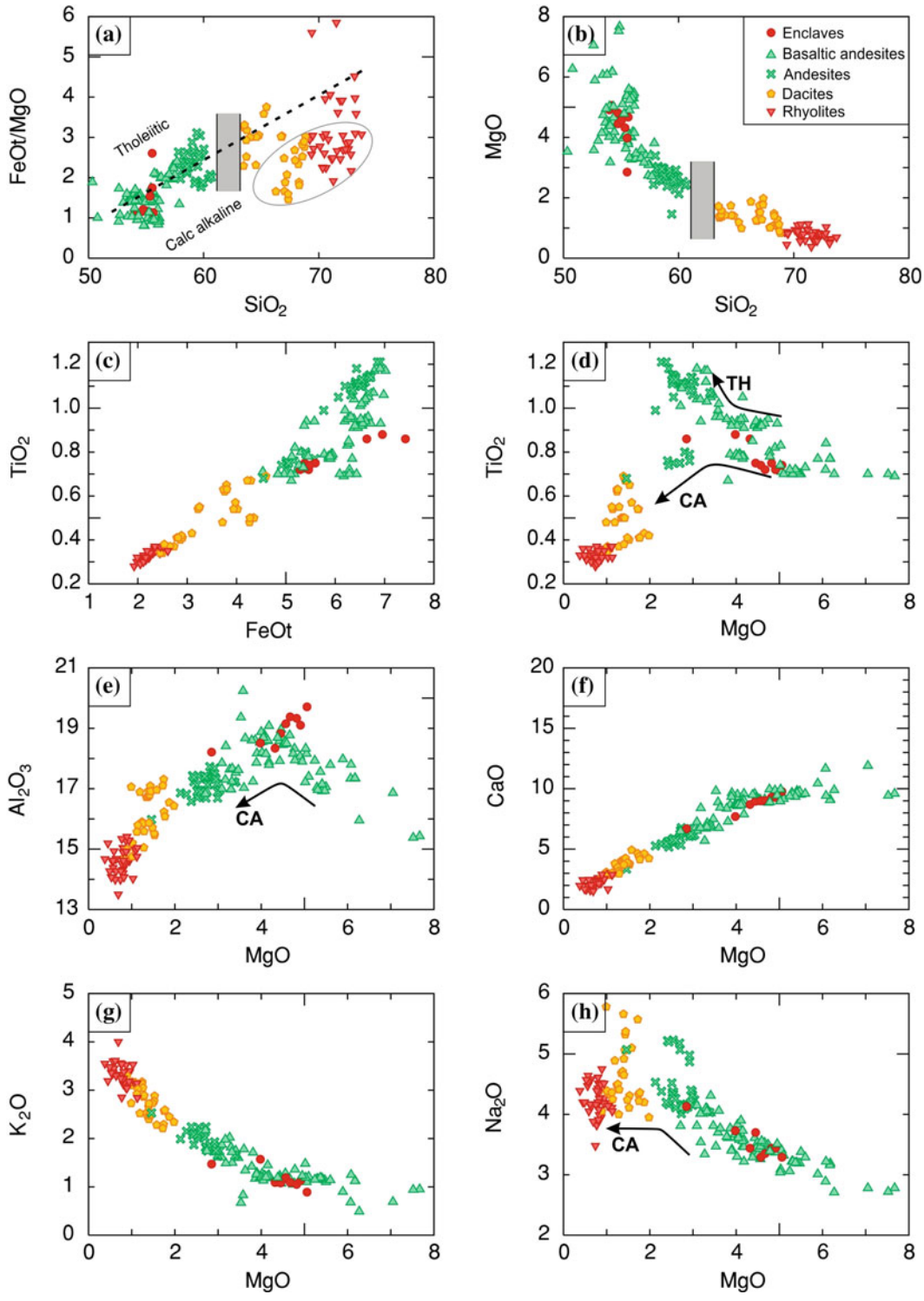
(a)
FeOt/MgO
SiO2
Tholeiitic
Calc alkaline
(b)
MgO
SiO2
Enclaves
Basaltic andesites
Andesites
Dacites
Rhyolites
(c)
TiO2
FeOt
(d)
TiO2
MgO
TH
CA
(e)
Al2O3
MgO
CA
(f)
CaO
MgO
(g)
K2O
MgO
(h)
Na2O
MgO
CA

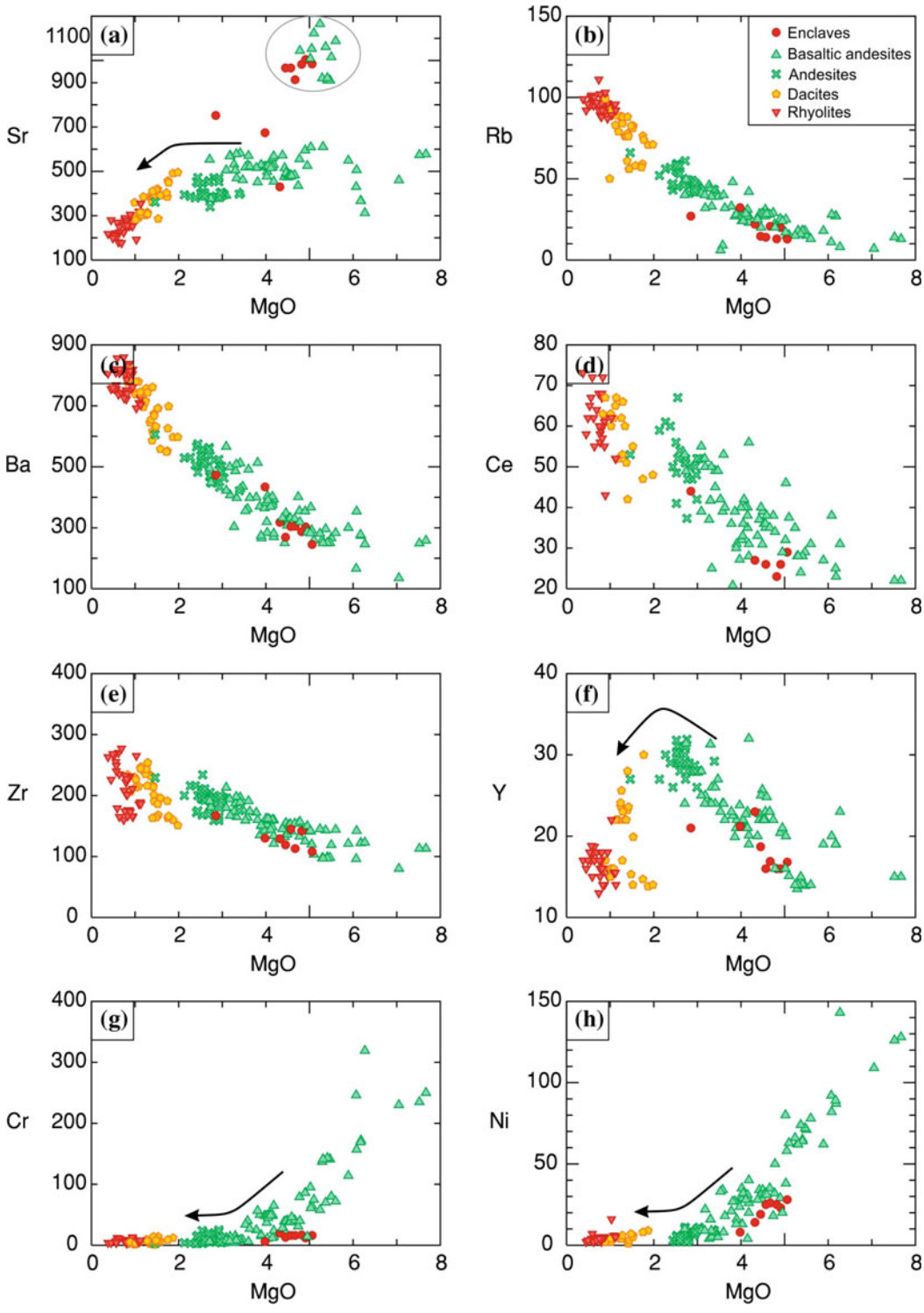

Fig. 4.22 Bulk rock composition of Nisyros volcanics: selected incompatible (Rb, Sr, Ba and Ce) and compatible trace elements (e.g. Ni, Cr, Zr, and Y) plotted against MgO. The calc-alkaline trend is marked with down- and up bending *arrows* in plots (**a**), (**f**), (**g**) and (**h**)

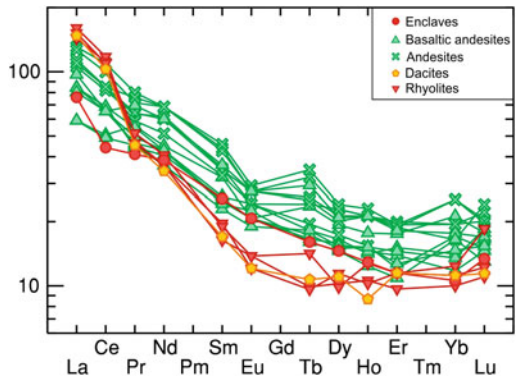

Fig. 4.23 Chondrite normalized rare earth element (REE) patterns (MacDonough and Sun 1995) of selected Nisyros lavas and enclaves (values in Electronic Supplementary Material Appendix)

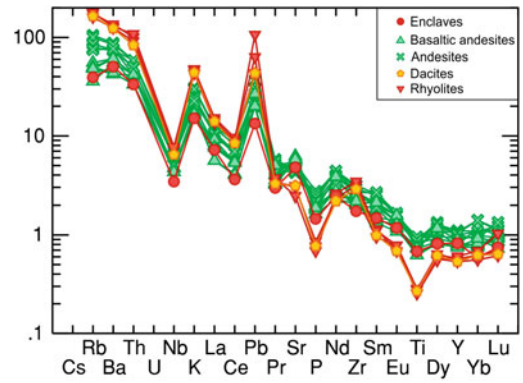

Fig. 4.24 Bulk chemical composition of Nisyros volcanics expressed as "multi-element variation diagram" of selected major and trace elements, normalized to normal N-type mid-ocean ridge (MORB) basalt composition (Sun and MacDonough 1989)

Table 4.5 Division into groups of chemical compositional variations of basaltic andesites and andesites of Nisyros pre-caldera lavas from Units No. 1 and 2

Rock type	Basaltic andesites			
Unit-sample	1 A-R192	1-B1	1-B2	1-C
wt%				
SiO_2	52.2	55.0–56.0	55.0–56.0	54.0–55.4
TiO_2	0.7	0.7–0.8	0.7–0.8	0.93–0.95
AI_2o_3	16.8	17.0–18.6	17.0–18.0	17.9–18.5
Fe_2O_3(t)	7.1	5.0–6.0	5.4–6.4	6.2–7.5
MnO	0.12	0.1	0.09	0.13
MgO	7.1	4.8–5.5	5.0–5.4	3.9–4.4
CaO	11.9	9.5–10.0	9.5–9.8	9.5–9.7
Na_2O	2.78	3.2–3.5	3.2–3.5	3.4–3.8
k_2O	0.69	1.07–1.17	1.1–1.7	1.22–1.29
p_2O_5	0.12	0.18–0.20	0.16–0.18	0.16
ppm				
Nb	n.d.	6	5.7–6.3	8–13
Zr	168	97–130	98–120	120–150
Y	n.d.	14	14	20–23
Rb	7	18–22	15–18	27–28
Sr	460	500–610	910–1050	500–530
Ni	109	32–62	62–72	13–24
Cr	230	50–140	65–140	11–24
V	200	140	140–143	167
Ce	n.d.	28	28	39
Ba	135	250–370	250–290	250–284
La	n.d.	13	13	14–15

Submarine volcanic base

Sources Rehren (1988), Wyers and Barton (1989), Seymour and Vlassopoulos (1992), Francalanci et al. (1995), Vanderkluysen et al. (2005), Zellmer and Turner (2007) and Spandler et al. (2012). *n.d.* not determined

Table 4.6 Bulk chemical composition of basaltic andesites and andesites from the LSU Nos. 3–24 of the early shield volcanic cycle (Nos. 3–11) and the composite stratovolcano cycles (Nos. 13–24)

Rock Type	Bas.And.	Andesite	Andesite	Bas.And.	Bas.And.	Bas.And.	Bas.And.	Bas.And.	Andesite	Bas.And.	Andesite	Bas.And.	Bas.And.	Bas.And.
LSU	3	4	5	6	8	10	11	13	15	16	19	21	22	24
Thickn. m	30	40	40	60	5	70	35	max. 40	max. 40	30	80	max. 15	max. 15	max. 25
wt.%														
SiO_2	53.3	56.0–57.8	55.7–60.0	51.7	53.7–56.7	54.3–55.7	52.7–57.7	54.0–60.0	58.5–59.7	53.3	60.0–61.2	54.2–58.8	54.0–59.0	53.0–59.5
TiO_2	1.05	1.18	1.17–1.0	0.76	0.83–1.23	0.69–0.78	0.77–1.04	0.92–1.2	1.11–1.15	0.7	0.7–0.8	0.72–1.12	0.8–1.2	0.78–1.16
Al_2O_3	18.58	17.4	17.7–16.8	16.9	17.9–17.1	17.9–15.4	18.8–16.8	18.6–16.8	17.4–17.0	16.5	17.5–18.0	17.6–16.7	18.7–16.6	18.8–16.9
Fe_2O_3(t)	7.36	7.4–7.2	7.8–6.4	3.24	6.9–7.9	6.9–5.9	7.0–7.35	6.0–7.7	7.16–7.46	6.3	5.6–6.2	5.9–7.3	5.9–7.7	6.0–7.5
MnO	0.12	0.10	0.13	0.09	0.12	0.0–0.11	0.13	0.11–0.14	0.12–0.14	0.11	0.12	0.09–0.13	0.09–0.14	0.11–0.13
MgO	4.15	3.3–2.4	3.3–2.1	1.56	6.1–2.7	7.7–4.8	5.9–2.7	4.4–2.25	3.0–2.5	6.8	2.5–3.2	6.18–3.0	5.24–2.38	4.9–2.2
CaO	9.08	5.7–5.2	7.2–5.3	10.57	9.5–6.3	9.6–9.0	10.4–6.5	9.05–5.3	6.8–5.9	1014	5.8–6.3	9.3–6.1	9.4–5.44	9.8–5.7
Na_20	3.47	3.3–4.2	4.1–4.5	2.20	3.1–3.9	2.7–3.3	3.0–4.1	3.4–4.4	4.0–4.5	2.84	4.8–5.3	3.2–4.2	3.06–4.20	3.4–4.3
K_2O	1.45	1.9–2.0	1.5–2.2	1.86	1.2–1.7	0.94–1.48	0.9–2.2	1.5–2.2	1.8–2.1	0.5	1.9–2.1	1.12–1.75	1.14–2.24	1.13–2.15
P_2O_5	0.23	0.25	0.25–0.30	0.20	0.2–0.25	0.14–0.19	0.18–0.3	0.21–0.28	0.25–0.27	0.48	0.23–0.25	0.18–0.25	0.18–0.30	0.19–0.26
ppm														
Nb	14	13–16	13–17	13	10–13	6–8	9–14	Dec–17	14–17	8	n.d.	6–14	6–17	10–16
Zr	148	174–200	165–235	156	140–174	113–144	145–194	150–216	180–210	123	159–175	120–200	140–215	125–200
Y	23	25	26–31	21	20–30	14–16	20–24	22–30	31–29	23	n.d.	15–28	14–29	20–36
Rb	31	43–46	33–59	61	24–37	13–20	18–40	27–56	43–55	8	41–47	16–44	15–57	27–59
Sr	559	530–470	470–395	404	610–430	575–1090	550–570	570–340	380–405	312	450–470	1060–400	1165–380	595–400
Ni	4	4	3	6	82–18	128–50	62	34–5	8–2	143	3–10	90–9	66–9	30–<3
Cr	12	4	3	16	157–10	250–40	114	39–3	9–5	319	14–24	170–5	58–3	86–25
V	172	230–150	230–140	117	240–175	140–155	170–100	180–215	220–195	160	100–135	170–210	130–230	160–210
Ce	40	37–50	25–67	46	29–46	22–34	27–53	37–61	48–56	31	n.d.	23–52	35–60	30–45
Ba	385	300–480	400–550	400	286–400	250–320	300–500	320–535	465–535	246	500–565	275–480	280–565	275–505
La	20	21–25	19–31	24	16–23	11–15	18–27	18–30	24–29	15	n.d.	12–26	16–34	14–24

Data sources Rehren (1988), Wyers and Barton (1989), Seymour and Vlassopoulos (1992), Francalanci et al. (1995), Vanderkluysen et al. (2005), Zellmer and Turner (2007) and Spandler et al. (2012).
n.d. not determined

SiO_2 contents range between 52 and 75.7 wt% (Electronic Supplementary Material Appendix Fig. 4.50), from basaltic andesite to rhyolite with dacites from 64 to 68 wt% and rhyodacites from 68 to approximately 70 wt%. Only two lavas of units 16 and 21 showed basaltic composition, with SiO_2 of 50 wt% and MgO of 6.3 wt%, and 3.5 wt%, respectively. The most primitive basaltic andesites have MgO contents of 7.0–7.7 wt% with SiO_2 contents that range from 52 to 55 wt% (Table 4.5). The samples that contain >5 wt% MgO are mafic enclaves. Al_2O_3 spans a range of 15.4 –18.5 wt%; it increases in the plagioclase rich basaltic andesites and decreases progressively from the andesites through dacites and rhyolites. FeO_{tot} and TiO_2 decrease as MgO decreases (e.g., Fig. 4.21c, d), while K_2O and Na_2O show the opposite trend (Fig. 4.21g, h).

The major element data shows a silica gap from 61.5 to 64.0 wt%, between andesites and dacites (Fig. 4.21a, b). The discontinuity in MgO and TiO_2 trends roughly coincides with the occurrence of the silica gap. Taking into account the petrographic observations in dacitic lavas, such as contamination with xenocrysts and millimetre size andesitic enclaves, the gap might actually be larger, as postulated by Wyers and Barton (1989) and Seymour and Vlassopoulos (1992). Mingling and mixing effects are clearly reflected by the lower values of FeO_{tot}/MgO for dacites, rhyodacites and rhyolites (encircled in Fig. 4.21a), which results from the random amount of enclaves and xenocrysts.

K_2O typically ranges between 1 and 3 wt%, but reaches as high as 4 wt% in some rhyolitic samples. It fits and overlaps the potassium array of all other calc-alkaline suites of the South Aegean volcanic arc (Mitropoulos et al. 1987; Pe-Piper and Piper 2002). However, glass microprobe analyses range from 3 to 4 wt% K_2O in the Argos and Nikia rhyolites (Units Nos. 17 and 30) and in the post-caldera rhyodacites (unit No. 32), reaching up to 6 wt% in some samples. The sodium content scatters within the dacitic compositions, whereas it decreases within the high-silica rhyolites.

The variations in selected trace element abundances are shown on the MgO diagrams in Fig. 4.22. The variation of the incompatible, large-ion lithophile elements (LILE) Sr, Rb, Ba is rather large with factors up to 4, whereas the high field strength elements (HFSE) Zr and Y vary only by a factor of 2.7.

Ba and Ce (Fig. 4.22c, d) generally increase with decreasing MgO, Ce displaying significant scatter in the basaltic andesite compositions between 6 and 3 wt% MgO. Sr (Electronic Supplementary Material Appendix Fig. 4.52a) systematically increases with decreasing MgO from about 200 to over 500 ppm, followed by a bend at around 2 wt% MgO that marks a trend of decreasing Sr content in the dacites and rhyolites. Independently, several basaltic andesites and enclaves with MgO between 4.2 and 5.6 wt% contain high Sr values between 900 and 1100 ppm. The highly incompatible element Rb (Fig. 4.22b) varies by up to a factor of 10 for a given MgO content, but most of these variations are confined to the basaltic andesites. Zr varies by a factor of 3 over the entire compositional range, with larger variation for differentiated basaltic andesites (Fig. 4.22e). Y generally decreases in the dacites and rhyolites and thus follows the iron-titanium enrichment and subsequent decrease of the calc-alkaline trend (Fig. 4.21f). It does not show the arc tholeiitic trend expressed in the TiO_2/MgO variation diagram. Ni and Cr are positively correlated with MgO (Fig. 4.22g, h), decreasing from generally 200 ppm for Cr in basaltic andesites to values <3 ppm. Ni contents decrease from 100 to <3 ppm.

The low Nb contents, only shown in Tables 4.5, 4.7, 4.8 and 4.9 are typical for island-arc subduction related magmas.

Chondrite-normalized rare earth element (REE) patterns of selected Nisyros lavas and enclaves (Fig. 4.23) display moderate La/Yb ratios of 3.5 for basaltic andesites to highly fractionated ratios La/Yb > 10 for dacites and rhyolites. Light-rare earth elements (LREE) are enriched relative to the heavy-rare earth elements (HREE). Some of the more evolved samples are also depleted in Dy, Ho, and Er. Generally,

Table 4.7 Division of five groups from basaltic andesites to andesites on the basis of characteristic major and trace element contents, which constitute the flows and pyroclastic deposits of Units No. 21 and 22

	SiO_2	TiO_2	MgO	Cr	K_2O	Rb	Sr	Nb
A	54.4	0.78	6.2	170	1.12	27	500	10
B2	55.8	0.72	5.3	70	1.2	16	1060	6
c	54.8	0.93	4.5	40	1.2	25	480	11
D	58	1.1	3.3	6	1.7	28	400	14
E	58.8	1.2	2.4	5	1.8	29	450	17

Oxide values are listed in %, elemental values in ppm

almost all REE (i.e. Pr, Nd, Sm, Eu, Tb, Dy, Ho, Er, Yb, Lu) show increasing concentrations from the basaltic andesites to the andesites. In contrast, spoon-shaped depletion occurs in the middle REE (MREE) to heavy REE (HREE) patterns in the rhyolites and dacites.

Table 4.8 Compiled bulk chemical compositional variation of dacites in Unit 14* (Zellmer and Turner 2007), Units 18** and 19** (Rehren 1988; Vanderkluysen et al. 2005) from the Afionas tuff cone, and Unit 25*** from Emborios flows and dome (Francalanci et al. 1995; Volentik et al. 2005)

Rock type	Dacite flow	Dacite flow	Dacite pyroclastics	Dacite flow
Unit No.	14*	18** ***	19**	25* ***
wt%				
SiO_2	67	64.0–65.5	65–67	64.5–69.0
TiO_2	0.65	0.6–0.5	0.7–0.5	0.64–0.54
AI_2O_3	15.5	17.3–17.0	17.5–17.0	16.4–15.6
Fe_2O_3(t)	4.2	5.0–4.8	4.5–3.8	4.9–3.6
MgO	1.5	1.5–1.2	1.7–0.7	1.25–1.1
CaO	3.7	4.1–3.8	5.5–2.7	3.5–3.0
Na_2O	4.3	4.8–5.5	4.3–5.5	4.3–5.4
K_2O	2.9	2.5–2.6	1.9–2.8	2.7–3.2
ppm				
Nb	15	16	n.d.	17–19
Zr	168	195–240	190–240	235–255
Y	20	22	n.d.	18–24
Rb	83	76	44–78	80–88
Sr	286	385–396	300–490	300–320
Ni	6	<3	<3	4
Cr	14	2–14	<3	8–9
V	90	50–40	n.d.	48–50
Ce	n.d.	n.d.	n.d.	70
Ba	692	645–690	550–744	670–760
La	n.d.	n.d.	n.d.	36

Major- and trace element data are on water free basis

All four different types of dacites show overlapping compositions with very similar characteristics. However, the spread within the Afionas eruptive cycle seems to be larger than the earlier and later cycles, which is expressed by CaO, K_2O, Rb, Sr and Ba; *n.d.* not determined

Table 4.9 Compiled rhyolitic compositional variation of pyroclastics and lavas, which erupted during the "caldera– and post caldera cycles", compared to the Stavros Avlaki rhyolite of the "composite stratovolcano cycle"

Volcanic edifice	Lower pumice	Nikia flows	Upper pumice	Prof. Ilias domes, flows	Avlaki dome, flows
Unit	28	30	31	32	17
wt%					
SiO_2	74.5–75.5	69.3–74.8	69.2–72.66	66.3–70.35	70.3–73.2
TiO_2	0.34–0.31	0.37–0.32	0.38–0.30	0.43–0.32	0.37–0.28
AI_2O_3	14.6–13.9	15.5–14.5	15.45–14.35	16.5–15.1	14.2–14.9
Fe_2O_3(t)	2.50–2.30	3.1–2.5	3.0–2.55	3.4–2.5	2.7–2.3
MgO	1.05–0.64	0.95–0.45	1.3–0.60	2.0–0.9	0.95–0.64
CaO	1.75–1.57	2.6–2.0	3.2–2.3	4.3–2.9	2.54–2.0
Na_2O	4.7–4.3	4.6–4.25	4.5–4.0	4.8–4.0	4.–4.1
K_2O	3.5–4.1	2.9–3.5	2.9–3.6	2.35–3.15	3.2–3.54
ppm					
Rb	89–97	88–100	84–99	71–103	95–111
Sr	180–210	290–200	315–255	495–305	224–280
Ba	690–750	735–810	815–725	600–815	804–859
La	35–41	32–37	37–39	29–31	34
Ce	62–65	55–58	57–60	48–52	53
Zr	265–280	265–280	200–250	150–190	160–180
Nb	14–20	10–19	15–17	12–14	14–21
Y	18–20	22–17	16–18	14–30	17–13
Ni	<3–16	<3–2	<3–3	5–9	5
Cr	<3–12	2–20	4–17	5–12	10–13
V	19–18	40–18	31–20	57–32	34–27
Sr 87/86	0.70424	0.704539	0.70456	0.70432	n.d.

Major- and trace element data on water free basis from Francalanci et al. (1995) and Vanderkluysen et al. (2005); strontium isotope ratios from Francalanci et al. (1995)

The general bulk chemical island-arc type characteristics of selected lavas and their enclaves can clearly be recognized using a "multi-element diagram" (Fig. 4.24) of selected Nisyros volcanic rocks. A depletion in high field strength elements (HFSE) relative to REE is observed. In the highly differentiates rhyolites, incompatible elements are enriched while compatible elements are depleted.

The typical island arc characteristics are expressed in the enrichment up to ten times in low field strength elements (LFSE) such as K, Rb, Sr, Ba, Th, and the light rare earth elements (e.g. Ce) and to a lesser extent Sr, Hf and Zr. In contrast, the basalts are depleted in high field strength elements (HFSE), such as Zr, Nb, Ti, Y, and the heavy rare earth elements (e.g. Yb). The pattern of the basaltic andesites, andesites and that of the enclaves are very similar, which indicates the close magmatic relationship. Basaltic andesites, andesites and dacites have a pronounced positive Pb anomaly and negative Nb, Ce and P anomalies; dacites, rhyodacites and rhyolites show strong Nb, P and Ti anomalies.

The compositions of the intermediate and evolved lavas, such as the dacites and rhyodacites are enriched in Rb, Ba, Th and LREE up to a hundred times when compared to the MORB.

Positive correlation of K, Rb and Ba with Th is evident. This also holds for Nb, Zr, Hf, and the LREE, whereas the compatible minor and trace elements Cr (incl. Ni), V, and Sc display a negative correlation with Th. In this respect, the Nisyros lavas do not significantly differ from the younger 'Main Volcanic Series' on Santorini (Nicholls 1971, 1978; Mann 1983; Barton and Huijsmanns 1986; Mitropoulos et al. 1987; Huijsmans et al. 1988; Fytikas et al. 1990).

4.3.2 Early Nisyros Shield Volcanic Cycles

4.3.2.1 Submarine Volcanic Base

Lithostratigraphic Units (LSU) No. 1 and 2 that form the pillow lavas and hyaloclastites of the submarine volcanic base are composed of basaltic andesites. Four groups A, B1, B2, and C of varying differentiated chemical compositions can be recognized based on the available analyzed data (Table 4.5). It has to be noted that neither the exact lithostratigraphic position of these samples is known from the thick pillow sequence nor their exact position within each pillow. A smooth differentiation trend in the major (i.e. TiO_2 and K_2O increasing, MgO decreasing) and incompatible trace elements (i.e. Rb and Nb increasing, Cr and Ni decreasing) can be seen from A to C. The only exception is Sr in B2 with higher values. Oxide values are listed in %, elemental values in ppm.

4.3.2.2 Early Shield Volcanic Cycle

Within the "Early Nisyros Shield Volcanic Cycles" (*Units Nos. 3–11*) the lavas vary in composition from basaltic andesite to andesite. This variation is not correlated with the lithostratigraphic sequence (relative age) (Table 4.4). Some lavas can be divided into groups (Tables 4.5A–C and 4.7A–E) according to their bulk chemistry. Oxide values are listed in %, elemental values in ppm (Table 4.6). A comprehensive description of the bulk chemical characteristics of the individual lithostratigraphic units is given in the following paragraphs:

Unit No. 3: Basaltic andesite varies within the range of the pillow lava of the groups B and C of the submarine volcanic base (Units Nos. 1 and 2), slightly more differentiated; *Unit No. 4:* Lava of andesitic composition; *Unit No. 5:* The 40 m thick flows vary slightly in andesitic composition similar to Unit 4; *Unit No. 6:* There is only one analysed sample available for the 60 m thick basaltic andesite pyroclasic succession. It seems to be more differentiated than the older units, despite the lower SiO_2 of 51.7 vol.%.

4.3.2.3 Internal Lake-Stage and Associated Volcanic Cycles

Unit No. 8: The 5 m thick lava flow is of highly porphyritic basaltic andesite composition, similar to group B1, including a more differentiated level (Table 4.6). *Unit No. 10:* The 70 m thick lavas, wide spread within the caldera walls, are of rather primitive basaltic andesite composition, similar to group A (Table 4.5). Some samples seem to be slightly more differentiated and differ significantly in high Sr concentrations up to about 1090 ppm; *Unit No. 11:* The 35 m thick pyroclastic flow succession marks the end of the "Early Volcanic Cycles" and varies from basaltic andesite to andesitic composition. However, some levels are similar to group B1, Table 4.5).

4.3.3 Composite Stratovolcano Cycles

4.3.3.1 Transition from Shield- to Stratovolcano

Unit No. 13: The Lavas of the "Early Caldera Composite Stratovolcano Cycles" are mainly of andesitic composition, some levels seem to be slightly less differentiated basaltic andesites. A significant difference between unit No. 13 and the older andesitic lavas occurs in the strontium values; *Unit No. 14:* For the first time in the eruptive cycles of Nisyros Volcano a

25 m thick lava flow of dacitic composition occurs within the uppermost part of today's northern caldera wall. The outstanding characteristic is the large amount of andesitic enclaves, which generally reaches 30% of the total rock volume and in some cases even up to 70–80%. The composition of a sample, free of macroscopically visible enclaves is shown in Table 4.8. Unusual are the high Ba values; *Unit No. 15:* In the northern eastern parts of the caldera and outer slopes the dacites are followed by a 40 m thick andesitic flow, which is chemically very similar in composition with the andesitic rocks of unit No. 13.

4.3.3.2 Southern Eruptive Centers (M. Stavros—Avlaki)

Unit No. 16: The 30 m thick succession of surge and pyroclastic flows in the southern and southwestern lower caldera wall consists of rather primitive basaltic composition; *Unit No. 17:* 60 m of rhyolithic flows and domes cover the southern segment of the island. They are very homogeneous and they lack enclaves and lithic xenoliths (Table 4.9).

4.3.3.3 Eastern Eruptive Centers (Afionas—Lies)

Unit No. 18: Two large tuff cones are building up the eastern slopes of the composite stratovolcano. The base of the southern Afionas cone consists of a dacite flow, which is rather free of enclaves and less differentiated than the older dacite of unit No. 14. Its chemical composition is listed in Table 4.8); *Unit No. 19:* Within the lifetime of the Afionas tuff cone several eruption cycles occurred, which erupted in alternating sequences andesitic and dacitic pyroclastics. The andesitic composition is quite variable, which seems to be dependent of sample inhomogeneity (Table 4.6).

4.3.3.4 The Composite Stratovolcano

Units Nos. 21 and 22: The bulk chemical compositions of these two units (Table 4.6) have to be grouped together since the small flows and pyroclastic deposits (strombolian activity), listed in Table 4.7, are scattered around several small scoria cones, which are spread all over the island. According to the existing analyzed samples five groups can be distinguished. They differ in the degree of differentiation and in their primary chemical characteristics, i.e. high values of strontium and low values of titanium and niobium.

4.3.3.5 Terminal Cycle and Dome Collapse

Unit No. 24: This unit is represented by thin lava flows of basaltic andesite to andesitic composition, which may have erupted after a time gap, since they are separated from the older lithostratigraphic units in several localities by epiclastic deposits, indicating erosion and tectonic activity. A series of thin basaltic andesite lava flows cover the western slopes of the island. The chemical characteristics of the basaltic andesites are similar to the previous units No. 21 and 22 and listed in Table 4.7.

Unit No. 25: Since the beginning of the volcanic activity of Nisyros, this eruptive cycle produced the largest volume of dacitic lava flows and domes, with a max. thickness of 150 m, containing a few percent of andesitic enclaves and xenolithic material. The variable chemical composition is shown in Table 4.8.

4.3.4 Caldera Eruptive Cycles and Caldera Collapse

4.3.4.1 First Caldera Cycle

Unit No. 28: The Caldera Cycles started with a succession of rhyolitic pumice fallout, surges and pyroclastic flows ("lower pumice") showing a normal trend of differentiation (Table 4.9). *Unit No. 29:* The major components of the blocks and debris of the heterogeneous breccia (Unit No. 29) are rhyolitic fragments from the overlying flows of Unit No. 30.

4.3.4.2 Second Eruptive Cycle

Unit No. 30: This is characterized by the effusion of the Nikia lava flows and Parletia neck, with a wide range of rhyolitic compositions listed in Table 4.8. In the Le Maitre classification (Fig. 4.20) diagram, the composition of the

porphyritic rocks with a high proportion of phenocrysts and small proportion of xenocrysts and quenched andesitic enclaves starts in the dacitic field. The evolved composition relates mainly to glassy rocks with small proportions of phenocrysts. The final glassy matrix composition and the plagioclase-hosted melt inclusions yield SiO_2 average values of 77.5 and 75.8 wt% respectively, at very low values of TiO_2, $FeO_{(tot)}$, CaO, and MgO (Seymour and Vlassopoulos 1989).

The mafic quenched enclaves are listed in Table 4.10. The spread of their compositions indicate that they must have derived from different stages of magmatic differentiation due to variable magmatic processes, such as fractional crystallization, magma mixing and contamination (see Sect. 4.4 and Fig. 4.20). The latter seem to be indicated by the higher calcium and strontium values.

Unit No. 31: This second large eruptive cycle ("upper pumice") started after an unknown time gap and produced a 30 m thick succession of pumice fallout, surges and pyroclastic flows, the "upper pumice". The variation in composition (Table 4.8) overlaps with the composition of the voluminous rhyolitic lavas of unit 30 and might also reflect certain contamination through small xenocrysts and xenolithic material, as well as effects of magma mingling.

Table 4.10 Compiled bulk chemical compositional variation of mafic enclaves in unit No. 30 (Nikia flows) and No. 32 profitis Ilias domes and flows

rock type	Basaltic andesites	Basaltic andesites
Unit	30 Enclaves	32 Enclaves
wt%		
SiO_2	55.3–55.54	54–55.6
TiO_2	0.86	0.75–0.72
AI_2O_3	18.2–18.5	18.8–19.7
Fe_2O_3(t)	7.4–8.2	5.9–6.2
MgO	2.9–4.3	4.4–5.0
CaO	6.7–8.69	9.0–9.8
Na_2O	3.4–4.1	3.3–3.4
k_2O	1.1–1.6	0.9–1.2
ppm		
Nb	8–13	7–8
Zr	129–167	108–145
Y	21–23	16–17
Rb	22–32	13–20
Sr	430–750	910–1000
Ni	8–14	23–28
Cr	6–20	13–16
V	140–190	140
Ce	27–44	23–29
Ba	320–470	269
La	18–27	13–15

Major- and trace element data on water free basis from Francalanci et al. (1995), Vanderkluysen et al. (2005) and Zellmer and Turner (2007)

4.3.5 Post-caldera Eruptive Cycle

Unit No. 32: The surficial emplacement of domes (i.e. Profitis Ilias) in the western part of the caldera and effusion of thick southwestward-directed lava flows with a max. thickness of 600 m represents the last volcanic cycle of Nisyros Volcano. The bulk chemical composition (Table 4.8) varies over a wide range from dacite to rhyolite, which led to the designation of the name rhyodacite (in the map and in all descriptive parts). End-member compositions have been analyzed in plagioclase-hosted melt inclusion and residual interstitial glass with SiO_2 average values of 75 and 73 wt% respectively (Seymour and Vlassopoulos 1989). In general the lavas and domes seem to be less evolved than the glassy rich rhyolitic flows of unit 30 (Table 4.8). However, the reason might be simple due to the large amount of phenocrysts and high proportions of quenched enclaves, which vary in size from millimeter to decimeter (see Sect. 4.2).

The amount of enclaves seems to increase in time from northeast to southwest, the youngest domes and lavas containing the most (Gansecki 1991). All enclaves (Table 4.9) are basaltic andesites with a narrow range of chemical composition, but distinctly different from all other prior basaltic andesites (Table 4.6). Unusual are the higher aluminum and strontium contents at low titanium and yttrium values.

4.4 Isotopic Evidence of Crustal Assimilation and Contamination

A number of bulk-rock and mineral isotope studies have been performed on Nisyros samples in order to assess the effects of crustal assimilation, of subduction-related magmatic and fluid input, as well as of differentiation in magma reservoirs.

Potential contamination and assimilation could be achieved at high crustal levels through the addition of fluids and materials from the altered Quaternary volcano-sedimentary rocks or Neogene marls. At deeper crustal levels the main contaminants are the Mesozoic limestones, the ophiolitic mélange and the metamorphic rocks of the Alpine basement, encountered in the geothermal wells in the Nisyros caldera (Geotermica Italiana 1983, 1984; Marini et al. 1993).

Although a large number of non-radiogenic and radiogenic isotope measurements including $^{87}Sr/^{86}Sr$, $^{143}Nd/^{144}Nd$, $^{176}Hf/^{177}Hf$, lead and uranium isotope series exist (Gülen et al. 1987; Gülen 1990; Wyers and Barton 1989; Francalanci et al. 1995; Buettner et al. 2005; Zellmer and Turner 2007; Braschi et al. 2014), stable isotope data is still missing. On the basis of $^{87}Sr/^{86}Sr$ analysis, Wyers and Barton (1989) assumed crustal contamination and assimilation, which could be implied based on the occurrence of calc-silicate xenoliths and clinopyroxene xenocrysts in the basaltic andesites of the early submarine volcanic cycle (Spandler et al. 2012). It has been suggested that carbonate assimilation of the Neogene and Mesozoic basement rocks may release CO_2, which could form a free vapor phase due to the low CO_2 solubility of basaltic magmas (Spandler et al. 2012).

The variation of $^{87}Sr/^{86}Sr$ ranges from 0.703384 in a basaltic andesite of the composite stratovolcano cycle to 0.705120 in a dacite of the Afionas-Kyra cycle (Units Nos. 18 and 19); Table 4.4. Vanderkluysen et al. (2005) interpreted this as a result of the differentiation from basaltic andesite to rhyolite. However, when taking all available data into consideration, a correlation between differentiation and $^{87}Sr/^{86}Sr$ ratios becomes indistinguishable. The low $^{87}Sr/^{86}Sr$ ratios are interpreted as mantle-like values reflecting abundant hydrous fluids in the source (Buettner et al. 2005), excluding major contamination and assimilation of crustal components (Table 4.4; Fig. 4.25).

Generally, the isotopic variability of the South Aegean Volcanic Arc rocks changes from east to west. The lowest $^{87}Sr/^{86}Sr$ isotope ratios are encountered at Nisyros and Santorini (0.7033 and 0.70328 respectively) and are comparable with those measured at ocean-ocean subduction zones (Briqueu et al. 1986). Crommyonia volcano shows the highest ratio of about 0.713 (Pe 1975). An overview of the isotopic values measured at

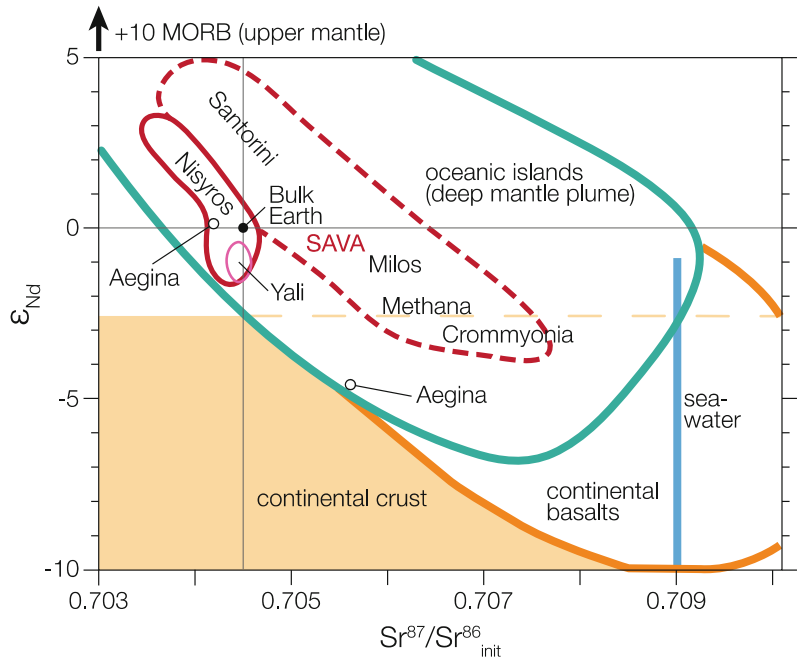

Fig. 4.25 Nd and Sr isotope variation for the South Aegean Volcanic Arc. Data from Pe (1975), Barton et al. (1983), Briqueu et al. (1986), Gülen (1987, 1990) Mitropoulos et al. (1998), Pe-Piper and Piper (2002), Buettner et al. (2005), Francalanci et al. (2007)

each volcanic island is given in Electronic Supplementary Material Appendix Fig. 4.55.

Further indicators of crustal assimilation appear in the range of neodymium isotope ratios (Buettner et al. 2005). $^{143}Nd/^{144}Nd$ ratios of the pre-caldera rhyolites (Unit No. 30) range between 0.512622 and 0.512675 (with values averaging at +0.2 E_{Nd}). Post-caldera (Unit No. 32) rhyodacites and the products of Yali Island (No.32) yield $^{143}Nd/^{144}Nd$ ratios between 0.512553 and 0.512607 (with E_{Nd} values averaging around −1.2). However, the Nisyros Nd isotope data is less radiogenic than the typical E_{Nd} of normal N-type MORB, averaging +10. This is in agreement with $^{176}Hf/^{177}Hf$ ratios. Whilst pre-caldera units range between 0.282914 and 0.282940 (with E_{Hf} values around +5.4), the post-caldera volcanics scatter between 0.282794 and 0.282917 (with less radiogenic E_{Hf} values of +2.4) compared to the typical E_{Hf} of N-MORB of +17. Thus, both Nd- and Hf-isotope systematics clearly indicate assimilation of crustal material, which is more apparent in the Yali and in the post-caldera volcanics. In addition, $^{206}Pb/^{204}Pb$, $^{207}Pb/^{204}Pb$ and $^{208}Pb/^{204}Pb$ ratios of Nisyros and Yali volcanic rocks support mixing of mantle material with a lower crust equivalent (Buettner et al. 2005).

Based on U–Th isotopic data (Zellmer and Turner 2007), the post-caldera rhyodacites (No. 32) have been interpreted as a remobilized magma from a young igneous protolith, activated by an influx of fresh mafic magma. In general, all rocks show small ^{238}U excess of up to ca. 10%. Mafic enclaves show higher U/Th ratios than their evolved host lavas, eliminating the simple fractionation hypothesis.

4.5 Petrogenetic Evolution of the Nisyros Volcanic Rocks

4.5.1 Introduction

The magmatic evolution of the Nisyros volcanics is inferred from mineralogical, petrologic and geochemical observations. Since the 1970s numerous petrogenetic models were proposed,

including various differentiation processes of mantle-derived, hydrous, calc-alkaline and arc tholeiitic basaltic magmas to generate evolved intermediate to silicic magmas. Fractional crystallization involving olivine, clinopyroxene, calcic-plagioclase, amphibole, biotite and Ti-magnetite at deep crustal magma reservoirs is regarded as the major differentiation mechanism (Bowen 1928). In particular, early crystallization of amphibole drives the differentiated magmas to dacitic, rhyodacitic and even to peraluminous tonalitic compositions (e.g. Cawthorn et al. Cawthorn and O'Hara 1976; Hürlimann et al. 2016).

In the case of Nisyros, the presence of xenoliths, reversely-zoned phenocrysts of plagioclase, clinopyroxene, amphibole and bulk rock trace element and isotopic characteristics led to the interpretation of multiple differentiation processes besides fractionational crystallization, such as crustal assimilation (AFC), magma mixing and mingling, and crystal retention-crystal-liquid-segregation. The role of crustal assimilation and contamination throughout the volcanic cycles has been recognized not only in the presence of xenocrysts and lithoclasts of the carbonate-rich basement rocks and their contact metamorphic equivalents, but also in the bulk chemical trace element and isotopic variations (Di Paola 1974; Limburg and Varekamp 1991; Seymour and Vlassopoulos 1992; Francalanci et al. 1995, 2005; Buettner et al. 2005; Vanderkluysen et al. 2005; Zellmer and Turner 2007; Spandler et al. 2012). Magma mingling and mixing between basaltic andesites and rhyolitic end-members generated dacites and rhyodacites, as suggested on the basis of mineral chemistry (plagioclase zonations), micro-textures and incompatible trace element systematics (Seymour and Vlassopoulos 1989, 1992; Zouzias and Seymour 2014). Using U–Th and Sr–Nd isotope systematics, Zellmer and Turner (2007) suggested remobilization of a young igneous protolith by injection of hot basaltic magma in order to produce dacitic melts.

4.5.2 The Depth of Magma Reservoirs, Amphibole Stability Fields and Ascent of Magmas Through the Crust

Several volcanological and petrologic characteristics of Nisyros Island allow an interpretation of the depth and origin of the magmas:

- The formation of a caldera with a diameter of 4 km points to the presence of a magma reservoir at shallow crustal depth between 3 and 7 km from which the highly differentiated rhyodacitic to rhyolitic magmas erupted.
- The existence of an active hydrothermal system indicates that cooling magma bodies at present are responsible for conductive and convective heat transfer.
- The existence of high-temperature brines has been proven by two deep geothermal wells, Nis-1 and Nis-2, reaching a maximum depth of 1816 m and 1547 m, respectively.
- The presence of Magnesium-rich hastingsitic amphiboles as xenocryst phases in the lavas and in the magmatic enclaves in dacites and rhyodacites indicate emplacement of mafic magmas from deeper crustal levels into a shallow crustal reservoir.
- The common presence of breakdown reaction rims on hastingsitic amphiboles testifies either heating by recharge with hot mafic melts or decompression during ascent through the crust.
- Olivine-rich hornblende-gabbro and pyroxenitic cumulates, however rare, point to an existence of deeper crustal reservoirs.

Mg-rich hastingsitic amphibole and anorthitic plagioclase are present in various proportions as the major phenocryst phases in most of the lavas in the volcanic islands of the South Aegean Volcanic Arc and therefore play a key role with respect to fractional crystallisation and mixing processes (Huijsmans et al.

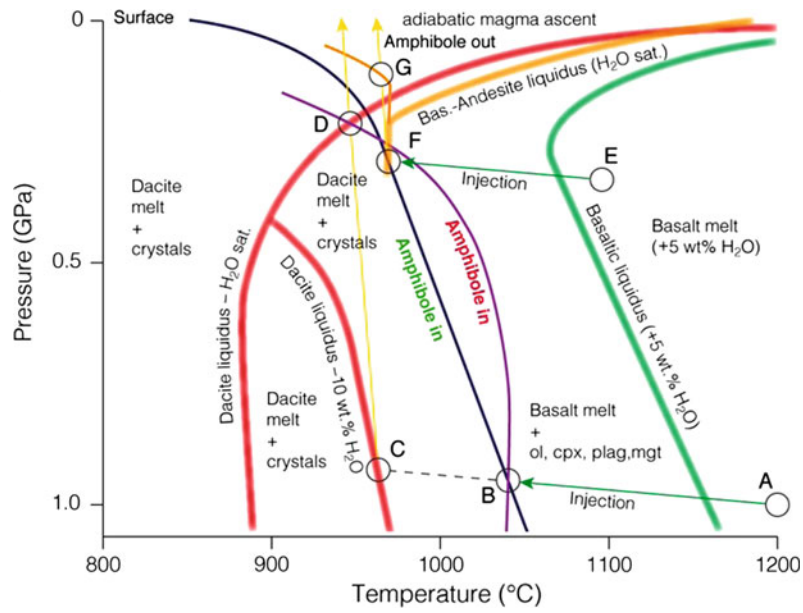

Fig. 4.26 The behaviour of water-bearing calc-alkaline magmas in the crust with regard to the stability fields of amphibole. Basalt liquidus with 5% H_2O (Foden and Green 1992), water-satured basaltic andesite (Moore and Carmichael 1998), dacite water-saturated with 10 wt% H_2O liquidus (Annen et al. 2006)

1988; Dietrich et al. 1988; Wyers and Barton 1989; Mitropoulos et al. 1987; Seymour and Vassolopoulos 1992; Mitropoulos and Tarney 1992; Francalanci et al. 1995; Gartzos et al. 1999).

Magnesio-hastingsites, pargasites, and ferroan pargasites, which have been found in the Nisyros gabbroic cumulates (Table 4.2) crystallised from water-rich melts of basaltic to andesitic composition. The stability fields of calcic-amphiboles vary over a wide pressure range of about 1–20 kbar and over a temperature range of up to 950 °C (Schmidt 1992). According to Ridolfi and Renzulli (2012), magnesio hornblendes and tschermakitic pargasites crystallize in equilibrium with calc-alkaline melts at low P, T conditions of up to 3kbar and within a range of temperatures between 800 and 920 °C, whereas magnesio hastingsites and pargasite are spread over a large field of pressures up to approx. 20 kbar and temperatures of 950–1100 °C. These results were confirmed by Nandedkar et al. (2014). Thus, the magnesio-hastingsites and pargasites of Nisyros may have crystallized in deep seated crustal magma reservoirs while magnesio-hornblendes and actinolitic hornblendes with Al_2O_3 = 6.5–7.1 wt% may have crystallised during the ascent of the rhyodacitic and rhyolitic melts and within shallow magma reservoirs.

The PT-diagram (Fig. 4.26) should illustrate the results of experimental research with regards to the stability field of amphiboles in water-bearing calc-alkaline magmas ascending from the upper mantle through the crust (review articles in Ulmer 2001; Müntener et al. 2001; Annen et al. 2006; Krawczynski et al. 2012; Dessimoz et al. 2012; Ridolfi et al. 2010; Ridolfi and Renzulli 2012; Nandedkar et al. 2014; De Angelis et al. 2015; Hürlimann et al. 2016).

The lower green arrow shows the injection of basaltic magma into lower crust (e.g. 25–30 km depth) from point A to B. Crossing the basaltic liquidus (+5 wt% H_2O), olivine, clinopyroxene, titanomagnetite and plagioclase start to crystallize along the path, forming orthocumulates. At point B amphibole starts crystallizing instead of clinopyroxene with adcumulate texture. At point C dacitic (or rhyolitic) residual melt is extracted by crystal fractionation from the basaltic melt remaining at depth or ascending adiabatically.

Between C and D the dacitic melt ascents through the liquidus field and thus any entrained crystal may be resorbed. At point D the melt

passes the liquidus and starts to crystallize but outside the amphibole stability field.

Path E to F shows a basalt melt injection and fast cooling into the upper crust that crystallizes olivine, clinopyroxene, titanomagnetite and plagioclase until amphibole appears at point F at the expense of clinopyroxene. During an adiabatic ascent the extracted differentiated basaltic andesite melt crystallizes amphibole until it reaches the stability boundary at point G, at high crustal levels. Here it leads to the crystallization of gabbroic and dioritic intrusives or to the extrusion of basaltic andesite and andesitic melts containing partly resorbed amphibole phenocrysts or cumulate relicts.

4.5.3 Magmatic Processes

The magmatic processes responsible for the evolution of Nisyros Volcano have been discussed by Wyers and Barton (1989) and Francalanci et al. (1995) on the basis of major and trace element chemical and isotopic composition of lavas and mineral chemistry.

A multi-stage pragmatic model (Fig. 4.27) has been chosen to demonstrate in a simple way the major magmatic processes, which control the petrogenetic evolution of magmas in crustal reservoirs. This model is coupled with the magma emplacement mechanisms at depth and

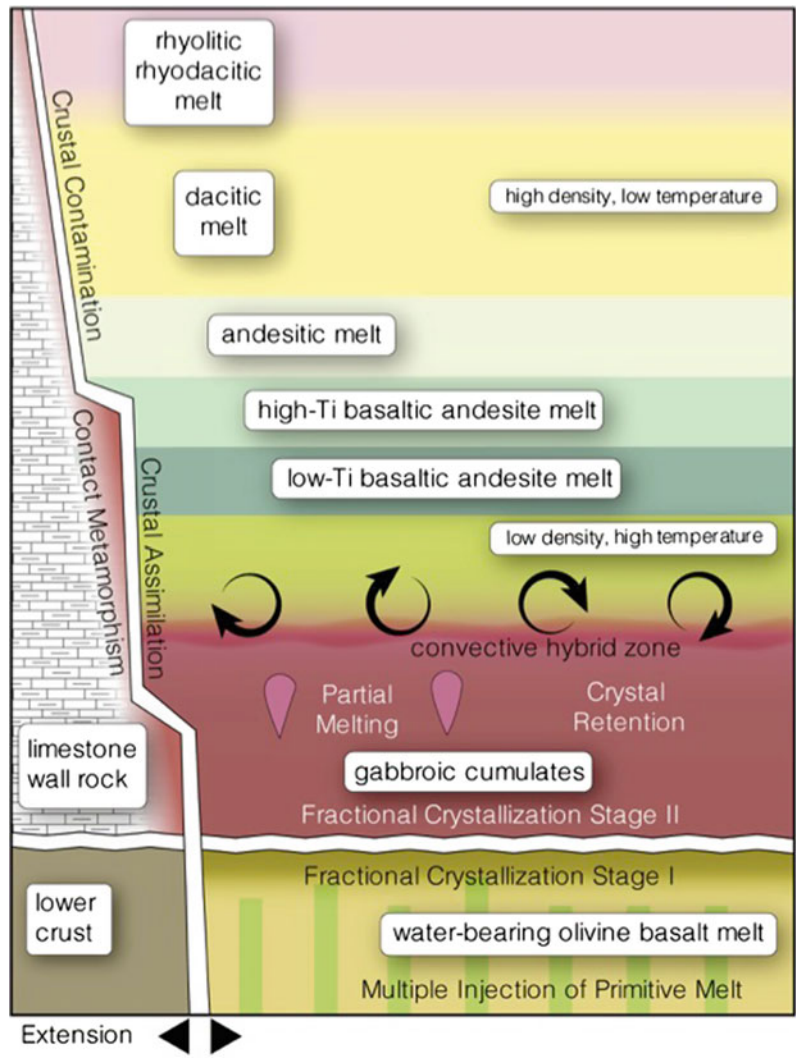

Fig. 4.27 Multi-stage model of a layered magma reservoir in the crust. Two steps of fractional crystallization, crustal assimilation, partial melting of cumulates and crystal retention are discussed as major magma differentiation processes in the text (modified after Dietrich et al. 1988)

its eruption at the surface and consists of two stages of fractional crystallization.

4.5.3.1 Fractional Crystallization

Stage I: Early fractional crystallization from primitive hydrous Mg-rich basaltic melts

Primary calc-alkaline and arc tholeiitic basaltic melts in volcanic island arcs may have originated by partial melting from a rather depleted mantle wedge of harzburgitic composition at approximately 120–130 km depth. Such a mantle is enriched in water and in the hygromagmatophile elements K, Rb, Ba, Sr, Th, U, and LREE, derived from the breakdown of subducted high-pressure phases (antigorite, phlogopite etc.), from altered and metamorphosed oceanic crust (e.g. Davies and Stevenson 1992; Sisson and Grove 1993a, b; Ulmer and Trommsdorff 1995; Tatsumi and Eggins 1995; Ulmer 2001). During ascent through the lithosphere and most probably at the mantle-crust boundary, the primary magmas underwent high-pressure fractional crystallization of olivine, clinopyroxene, amphibole and Cr-spinel under an open system and oxygen buffered conditions (e.g. Osborn 1976; Osborn and Rawson 1980; review in Annen et al. 2006). Experimental studies confirm such an assumption (Grove et al. 2002, 2005 and 2005; Nandedkar et al. 2014; Hürlimann et al. 2016).

Therefore, parental olivine basalts, generated from a primary hydrous basaltic melt, are seen as a first stage of crystal fractionation (Fig. 4.27). So far, no olivine basalts have been found on Nisyros Island. An early stage I fractionation process can only be inferred to some other cases in the South Aegean Volcanic Arc, e.g. lavas in the islands of Santorini, Aegina, and Methana.

Stage II: Fractional crystallization and assimilation

Wyers and Barton (1989) showed that crystal fractionation played a major role in the differentiation of Nisyros magmas, and implied that the compositional gap between basaltic andesites and dacites could not be explained by a simple isobaric fractionation. They concluded that the higher abundance of olivine in the andesites compared to the basaltic andesites could only be achieved by polybaric fractionation processes from variable parental magmas.

Francalanci et al. (1995) tried to explain the "jumps in the degree of evolution present in the stratigraphic series, accompanied by changes in the porphyritic index", in a simplified magma reservoir not through fractional crystallization, but through mechanisms of convection, assimilation, crystallization and crystal retention, combined with resorption and accumulation of major phenocryst phases (plagioclase and clinopyroxene).

Taking these possible complex magmatic differentiation processes under non-equilibrium conditions into consideration, a compositionally layered magma reservoir can be envisaged. Disturbances within an inversely layered system, variable in density, temperature and sensitive to convection and turnover, can easily be generated by injection of subsequent hot and less dense hydrous fresh melt.

Breakdown reactions of amphibole may contribute significantly to the amount of fluids. Assimilation of carbonate rocks bordering magma reservoirs may also release fluids rich in hygromagmatophile elements like strontium and light rare earth elements (LREE) into the melts. Pelitic rocks can release aluminum, potassium and rubidium.

The least differentiated lavas of Nisyros Volcano, which can be used as parental melt for the fractional crystallization model (Fig. 4.27), have been found in the basaltic andesites from units No. 10 and No. 16, inner caldera wall at Kato Lakki and Stavros, respectively (samples AV7B and AV24B, Table 4.5, Vanderkluysen et al. 2005, in wt%).

Important phases that control fractionation processes at stage II are olivine, anorthitic plagioclase, clinopyroxene, orthopyroxene, Fe–Ti oxides and Mg-rich amphiboles, the latter already occurring as early cumulate phases (e.g. adcumulates, Sect. 4.2.5). Basaltic andesites, andesites and evolved dacitic to rhyolitic melts are differentiation products depending on temperature and pressure conditions, the amount of fluids (oxygen fugacity) and the proportions of the fractionating phases.

4.5.3.2 Generation of Evolved Silicic Melts from a Parental Basaltic Andesite Magma

Major oxide modeling should give realistic solutions to derive dacitic and rhyolitic melts by fractional crystallization of plagioclase, olivine, clinopyroxene, Mg-rich amphibole and titanomagnetite. The fractionation of these minerals, in particular amphibole drastically changes the composition of the remaining melt by extracting Mg, Ti, Fe, Al, Ca and other elements, driving the remaining melt to a silicic composition. The most satisfactory model calculation leads to the generation of a rhyolitic magma (Table 4.11). The differences between calculated and natural TiO_2, K_2O, and Na_2O concentrations can be explained by the lack of Fe–Ti oxide data and the variation of alkali compositions in the basaltic andesites and rhyolites, respectively. Of course, such a model assumes fractionation from a single parental magma under equilibrium conditions. The mobilisation of rhyolitic melt can leave large volumes of amphibole-rich cumulates and gabbros behind. The gabbroic and dioritic clots found in the evolved magmas are witnesses of such processes

Least-squares mixing calculations (Bryan et al. 1969) were performed to test the effects of Mg-rich amphiboles included in the stage II fractional crystallization. Fractionation from a parental high-Mg basaltic andesite magma (e.g. Stavros lavas, Unit No. 16, Table 4.6) of the minerals found in the grabbro cumulate xenolith from the Lower pumice deposit (Unit No. 28) should generate either a residual dacitic or a rhyolitic melt.

The model calculation shows that approximately 65 wt% hornblende gabbro cumulate should crystallize from a basaltic andesite melt in order to generate 35 wt% rhyolitic melt, which implies the existence of large plutonic volumes at depth.

Recent fractional crystallization experiments by Nandedkar et al. (2014) with temperatures from a near-liquidus interval at 1117 °C to near-solidus temperature at 700 °C at a pressure of 0.7 GPa confirmed the fractionation model based on petrographic and geochemical evidence. About 40 wt% of ultramafic plutonic rocks have to crystallize to generate basaltic–andesitic liquids, and an additional 40 wt% of amphibole–gabbroic cumulate to produce granitic melts.

Table 4.11 Cumulative mineral and rock proportions (wt%) obtained by least-squares fractionation modelling

Sample	AV24B	Amp 15	0111	Cpx 11	Pig 12	Ti-mgt	Rhyolite	BasAnd.C.
Unit	16	28	28	28	28	0	30	
SiO_2	54.86	43.23	38.09	50.91	45.77	0.49	71.54	54.85
TiO,	0.74	3.33	0.06	0.71	0.05	2.32	0.33	1.02
AI_2O_3	16.96	12.88	0.02	3.80	34.53	2.89	14.70	16.98
FeO(t)	6.50	9.84	20.58	5.76	0.48	89.26	2.45	6.49
MgO	6.91	15.57	40.76	15.66	0.05	4.49	0.78	6.92
CaO	10.52	11.99	0.14	22.73	17.81	0.28	2.45	10.52
Na_2O	2.89	2.76	0.04	0.26	1.21	0.00	4.31	2.43
K_2O	0.51	0.34	0.00	0.00	0.10	0.00	3.43	1.06
Total	99.89	99.93	99.69	99.83	100.00	99.72	100.00	
Modes		32.85	0.44	9.94	21.09	2.17	36.46	
Errors		22.88	6.06	6.66	6.57	0.92	3.24	
R2	0.735							

Basaltic andesite (Stavros lava, Unit No. 16, recalculated to water free composition)—(Olivine Fo_{77}, plagioclase, clinopyroxene, amphibole, Ti-magnetite) = rhyolite (average Nikia lavas, Unit No. 30). *R2* residual squared from the linear regression

4.5.3.3 Magma Mingling and Mixing

Magma mixing is understood as a homogenisation process involving at least two magmas of different chemical compositions and rheology (McBirney 1980). Often it might be the subsequent step following magma mingling.

Magma mingling applies in particular to the Main Caldera and Post Caldera Eruptive Cycles. Examples of mingling are given in previous chapters and shown on Fig. 4.13 for the dacitic lavas No. 14 and on Fig. 4.14 for the rhyodacitic lavas No. 32.

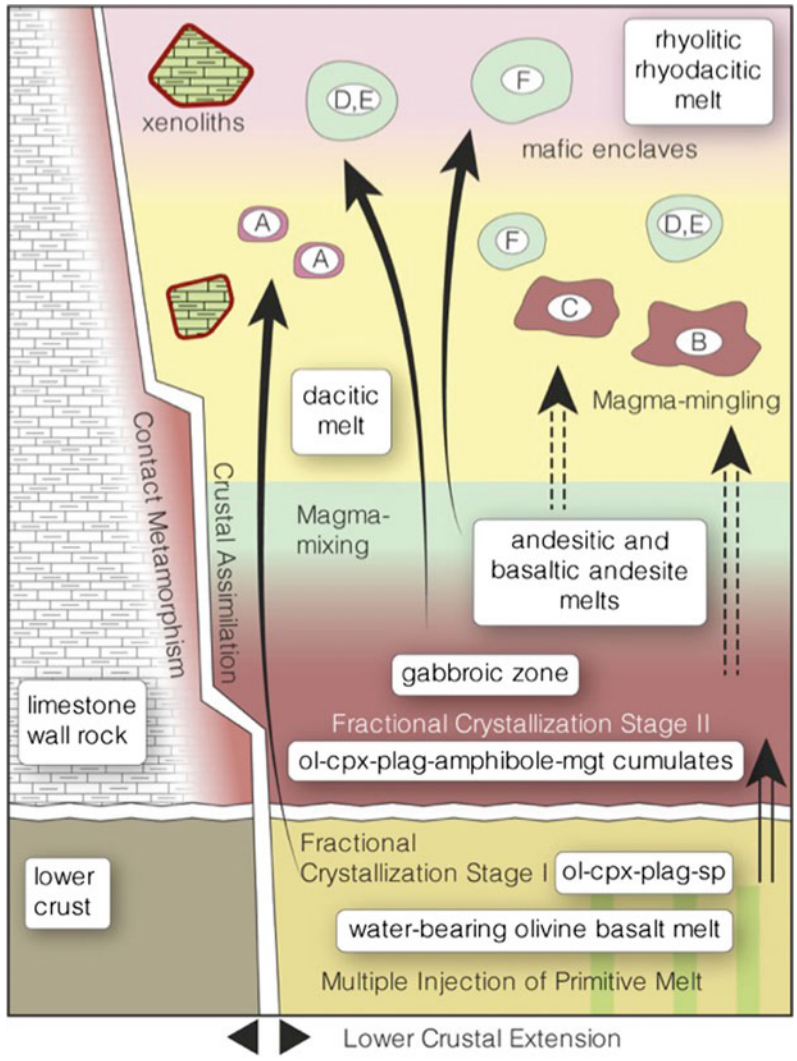

Fig. 4.28 Schematic model of magma mixing and mingling processes within magma reservoirs, independent of depth (figure modified after Dietrich et al. 1988). The capital letters denote the following inclusions in dacitic, rhyodacitic, and rhyolitic melts: *A* small cumulate crystals (e.g. Fo-rich olivine and spinel) from an early fractionation stage I; *B* and *C* clots of large cumulate xenoliths from a later fractional crystallization stage II, partially resorbed and molten; *D* and *E* gabbroic and dioritic xenoliths from the igneous zone of the magma reservoir; *F* mafic enclaves from the layered zone of basic to intermediate melts; *red rims* indicate contact metamorphic xenolith from the border regions (i.e. roof) of the magma reservoir. Sedimentary xenoliths consist of limestone, marbles and skarn (e.g. albite/hedenbergite, pyroxenites, muscovite-bearing, biotite-bearing mafic assemblages). Xenoliths of metamorphic rocks, which are abundant in the pyroclastic unit of the nearby Yali islet, are very rare in the Nisyros rocks. Black arrows denote the pathways of the enclaves

Examples of magma mixing have been recognized in all lavas from basaltic andesites to rhyolites throughout the history of Nisyros Volcano (e.g. Seymour and Vlassopoulos 1989, 1992; Francalanci et al. 1995; Zouzias and Seymour 2014). Evidence of magma mixing involving basic melts consists of mingled enclaves, crystal clots, minuscule quenched mafic enclaves, inverse compositional zonation of plagioclase and disequilibrium textures of plagioclase and amphiboles (Figs. 4.28, 4.2 and 4.10 respectively). The compositions of the xenocrysts found in dacites are similar to those of the phenocrysts from the basaltic andesites and andesites, whereas the dacite phenocrysts are more or less similar to those found in the rhyolites.

The effects of magma mingling and inefficient magma mixing are also evident in the bulk rock chemical variation of the rocks, expressed as a scatter of major and trace elements (Sect. 4.4 and Figs. 4.20, 4.21, 4.22, 4.23 and 4.24), exceeding by far the analytical errors.

A significant melting process that can be regarded as a result of a mixing process may happen during the injection of fresh hot magma into a pre-existing magma reservoir. Oberhänsli et al. (1985, 1989) and Dietrich et al. (1987) have described the role of mixing induced partial melting in cumulates from the volcanic islands of Aegina and Methana, which led to the generation of hybrid high Ti- and Al andesites. Cumulate xenoliths with similar textural characteristics have not yet been found in the Nisyros lavas. However, basaltic andesites in the pre-caldera lavas of Nisyros with higher Ti- and Al-contents may imply such a process (Tables 4.5 and 4.6).

References

Annen C, Blundy JD, Sparks RSJ (2006) The genesis of intermediate and silicic magmas in deep crustal hot zones. J Petrol 47:505–539

Bachmann O, Deering CD, Ruprecht JS, Huber C, Skopelitis A, Schnyder C (2011) Evolution of silicic magmas in the Kos-Nisyros volcanic centre, Greece: a petrological cycle associated with caldera collapse. Contrib Mineral Petrol 163:151–166

Bacon CHR (1986) Magmatic inclusions in silicic and intermediate volcanic rocks. J Geophys Res 91:6091–6112

Barton M, Salters VJM, Huijsmans JPP (1983) S-isotope and trace element evidence for the role of continental crust in calk-alkaline volcanism of Santorini and Milos, Aegean Sea, Greece. Earth Planet Sci Lett 63:273–291

Barton M, Huijsmanns JPP (1986) Post-caldera dacites from the Santorini volcanic complex, Aegean Sea, Greece: an example of the eruption of lavas of near-constant composition over a 2,200 year period. Contrib Mineral Petrol 94:472–495

Boettcher AL (1977) The role of amphiboles and water in circum-Pacific volcanism. In: Manghnani MH, Akimoto S (eds) High pressure research application in geophysics. New York Academic Press, pp 107–125

Bohla M, Keller J (1987) Petrology of plinian eruptians of Nisyros Volcano. Hellenic arc. Terra Cognita 7:171

Bowen N (1928) The evolution of the igneous rocks. Princeton University Press, Princeton

Braschi E, Francalanci L, Tommasini S, Vougioukalakis GE (2014) Unrevaling the hidden origin and migration of plagioclase phenocrysts by in situ Sr isotopes the case of final dome activity at Nisyros Volcano, Greece. Contrib Mineral Petrol 167:988–1013

Briqueu L, Javoy M, Lancelot JR, Tatsumoto M (1986) Isotope geochemistry of recent magmatism in the Aegean arc: Sr, Nd, Hf, and O isotopic ratios in the lavas of Milos and Santorini—geodynamic implications. Earth Planet Sci Lett 80:41–54

Bryan WB, Finger LW, Chayes F (1969) Estimating proportions in petrographic mixing equations by least-squares approximation. Science 163:926–927

Buettner A, Kleinhanns IC, Rufer D, Hunziker JC, Villa IM (2005) Magma generation at the easternmost section of the Hellenic Arc: Hf, Nd, Pb and Sr isotope geochemistry of Nisyros and Yali volcanoes (Greece). Lithos 83:29–46

Cawthorn RG, O'Hara MJ (1976) Amphibole fractionation in calc-alkaline magma genesis. Am J Sci 276:309–329

Davies JH, Stevenson DJ (1992) Physical model of source region of subduction zone volcanics. J Geophys Res 97:2037–2070

Davis E (1967) Zur Geologie und Petrologie der Insel Nisyros und Jali (Dodecanes) Proc Akad Athen 42:235–252

Davis E, Gartzos E, Dietrich VJ (1998) Magmatic evolution of the Pleistocene Akrotiri volcanoes. In: Casale R, Fytikas M, Sigvaldasson G, Vougioukalakis GE (eds) The European laboratory volcanoes, proceedings of the 2nd workshop, 2–4 May 1996, Santorini, Greece, EUR 18161 EN. European Commission, Luxembourg, pp 49–67

De Angelis SH, Larsen J, Coombs M, Dunn A, Hayden L (2015) Amphibole reaction rims as a record of pre-eruptive magmatic heating: an experimental approach. Earth Planetary Sci Lett 426:235–245

Di Paola GM (1974) Volcanology and petrology of Nisyros Island (Dodecanese, Greece). Bull. Volcanol. 38:944–987

Dessimoz M, Muntener O, Ulmer P (2012) A case for hornblende dominated fractionation of arc magmas: the Chelan complex (Washington Cascades). Contrib Mineral Petrol 163:567–589

Dietrich V (1989) Intramagmatic pillowing. Terra 1 (1):278 (abstract)

Dietrich VJ, Mercolli I, Oberhänsli R (1987) The complexity of discontinous fractionation in water-bearing magmas. Program IAVCEI 3:407.

Dietrich VJ, Mercolli I, Oberhänsli R (1988) Dazite, high-alumina Basalte und Andesite als Produkte Amphibol dominierter differentiation (Aegina und Methana, Aegäischer Inselbogen). Schweiz Mineral Petrogr Mitt 68:21–39

Eichelberger JC (1980) Vesiculation of mafic magma during replenishment of silicic magma reservoirs. Nature 288:446–450

Ellis BS, Bachmann O, Wolff JA (2014) Cumulate fragments in silicic ignimbrites: the case of the Snake River Plain. Geology 42:431–434

Feeley TC, Dungan MA (1996) Compositional and dynamic controls on mafic-silicic magma interactions at continental arc volcanoes: evidence from Cordón el Guadal, Tatara-San Pedro complex, Chile. J Petrol 37:1547–1577

Foden JD, Green DH (1992) Possible role of amphibole in the origin of andesite: some experimental and natural evidence. Contrib Mineral Petrol 109:479–493

Francalanci L, Varekamp JC, Vougioukalakis G, Defant MJ, Innocenti R, Manetti P (1995) Crystal retention, fractionation and crustal assimilation in a convecting magma chamber, Nisyros Volcano, Greece. Bull Volcanol 56:601–620

Francalanci L, Vougioukalakis GE, Perini G, Manetti P (2005) A west–east traverse along the magmatism of the south Aegean volcanic arc in the light of volcanological, chemical and isotope data. Dev Volcanol 7:65–111

Francalanci L, Varekamp JC, Vougioukalakis GE, Innocenti F, Manetti P (2007) Is there a compositional gap at Nisyros Volcano? A comment on: magma generation at the easternmost section of the Hellenic arc: Hf, Nd, Pb and Sr isotope geochemistry of Nisyros and Yali volcanoes (Greece). Lithos 95(3–4):458–461

Fytikas M, Kolios N, Vougioukalakis G (1990) Post-Minoan volcanic activity of the Santorini volcano, volcanic hazard and risk forecasting possibilities. In: Thera and the Aegean World III, vol 2. The Thera Foundation, London, pp 183–198

Ganseki C (1991) Petrology of the domes and inclusions of Nisyros Volcano, Dodecanese islands, Greece. BA thesis, Wesleyan University, Middletown, CT, 97 pp

Garcia MO, Jacobson SS (1979) Crystal clots, amphibole fraction and the evolution of calc-alkaline magmas. Contrib Mineral Petrol 69:319–327

Gartzos E, Dietrich VJ, Davis E (1999) Amphibole-plagioclase fractionational crystallisation and magma mixing nas major differentiation processes in the Akrotiri volcanic complex, Santorini, Greece. Schweiz Mineral Petrogr Mitt 79:231–262

Geotermica Italiana (1983) Nisyros 1 geothermal well. PPC-EEC report, pp 1–106

Geotermica Italiana (1984) Nisyros 2 geothermal well. PPC-EEC report, pp 1–44

Girard G, Stix J (2009) Magma recharge and crystal mush rejuvenation associated with early post-collapse upper basin member rhyolites, Yellowstone caldera, Wyoming. J Petrol 50:2095–2125. doi:10.1093/petrology/egp070

Graham CM, Harmon RS, Sheppard SMF (1984) Experimental hydrogen isotope studies: hydrogen isotope exchange between amphibole and water. Am Miner 69:128–138

Grove TL, Parman SW, Bowring S, Price RC, Baker MB (2002) The role of an H_2O-rich fluid component in the generation of primitive basaltic andesites and andesites from the Mt. Shasta region, N California. Contrib Mineral Petrol 148:542–565

Grove TL, Baker MB, Price RC, Parman SW, Elkins-Tanton LT, Chatterjee N, Müntener O (2005) Magnesian andesite and dacite lavas from Mt. Shasta, northern California: products of fractional crystallization of H2O-rich mantle melts. Contrib Mineral Petrol 148:542–565

Grove TL, Elkins-Tanton LT, Parman SW, Chatterjee N, Müntener O, Gaetani GA (2005) Fractional crystallization and mantle-melting controls on calc-alkaline differentiation trends. Contrib Mineral Petrol 145:515–533

Guillong M, von Quadt A, Sakata S, Peytcheva I, Bachmann O (2014) LA–ICP–MS Pb–U dating of young zircons from the Kos-Nisyros volcanic centre SE Aegean arc. J Anal At Spectrum 29:963–970

Gülen L (1990) Isotopic characterization of Aegean magmatism and geodynamic evolution of the Aegean subduction. Proceedings of conference on international earth science colloquium on the Aegean region, Oct 1–6 (1990) Izmir/Turkey, vol 2, pp 143–166

Gülen L, Hart SR, Salters VJM, Wyers GP, Barton M (1987) Sr, Nd, Pb, isotopic constraints on the petrogenesis of the Aegean arc volcanics. Terra Cognita 7:170–171

Huijsmans JPP, Barton M, Salters VJM (1988) Geochemistry and evolution of the calc-alkaline volcanic complex of Santorini, Aegean Sea, Greece. J Volcanol Geotherm Res 34:283–306

Hürlimann N, Müntener O, Ulmer P, Nandedkar R, Chiaradia M, Ovtcharova M (2016) Primary magmas in continental Arcs and their differentiated products: Petrology of a post-plutonic dyke suite in the tertiary Adamello Batholith (Alps). J Petrol 57(3):495–534

Innocenti R, Manetti P, Pecerillo A, Poli G (1981) South Aegean volcanic arc: geo-chemical variations and geotectonic implications. Bull Volcanol 44:377–391

Krawczynski MJ, Grove TL, Behrens H (2012) Amphibole stability in primitive arc magmas: effects of temperature,

H_2O content, and oxygen fugacity. Contrib Mineral Petrol. doi:10.1007/s00410-012-0740-x

Leake BE (1978) Nomenclature of amphiboles. Am Mineral 63:1023–1052

Leake BE, Wooley AR, Arps CES, Birch WD, Gilbert MC, Grice JD, Hawthrone FC, Kato A, Kisch HJ, Krivovichev VG, Linthout K, Laird J, Mandarino JA, Maresch WV, Nickel EH, Rock NMS, Schumacher JC, Smith DC, Stephensen NCN, Ungaretti L, Whittaker EJW, Youzhi G (1997) Nomenclature of amphiboles: report of the subcommitee on amphiboles of the international mineralogical association, commission on new minerals and mineral names. Am Mineral 82:1019

Limburg EM, Varekamp JC (1991) Young pumice deposits on Nisyros. Greece Bull Volcanol 54(1):68–77

Lodise L (1987) Petrology and geochemistry of Nisyros Volcano (Dodecanese, Greece). MA thesis, Wesleyan University, Middletown CT USA: 245 pp

Longchamp C, Bonadonna C, Bachmann O, Skopelitis A (2011) Characterization of tephra deposits with limited exposure: the example of the two largest explosive eruptions at Nisyros Volcano (Greece). Bull Volc 73:1337–1352

Mann AC (1983) Trace element geochemistry of high alumina basalt—andesite—dacite—rhyodacite lavas of the main volcanic series of Santorini volcano, Greece. Contrib Mineral Petrol 84:43–57

Marini L, Principe C, Chiodini G, Cioni R, Fytikas M, Marinelli G (1993) Hydrothermal eruptions of Nisyros (Dodecanese, Greece)—past events and present hazard. J Volcanol Geotherm Res 56:71–94

Martin L (2008) The petrology and geochemistry of mafic volcanic units from Nisyros Volcano, Greece: implications for magma evolution in island arcs. Master thesis University Bewrne, 113 pp

McBirney AR (1980) Mixing and unmixing of magmas. J Volcanol Geoth Res 7:357–371

McDonough WF, Sun SS (1995) The composition of the Earth. Chem Geol 120:223–253

Mitropoulos P, Tarney J (1992) Significance of mineral composition variations in the Aegean Island Arc. J Volcanol Geotherm Res 51:283–303

Mitropoulos P, Tarney J, Saunders AD, Marsh NG (1987) Petrogenesis of Cenozoic volcanic rocks from the Aegean Island Arc. J Volcanol Geotherm Res 32:177–193

Mitropoulos P, Tarney J, Stouraiti C, Notsu K, Arakawa Y (1998) Sr isotopic variation along the Aegean Arc: constraints on magma genesis on the basis of new Sr isotope data. Bull Geol Soc Greece 32:215–224

Miyashiro A (1974) Volcanic rock series in island arcs and active continental margins. Am J Sci 274:321–355

Moore G, Carmichael ISE (1998) The hydrous phase equilibria (to 3 kbar) of an andesite and basaltic andesite from western Mexico: constraints on water content and conditions of phenocryst growth. Contrib Mineral Petrol 130:304–319

Müntener O, Kelemen P, Grove T (2001) The role of H_2O during crystallization of primitive arc magmas under uppermost mantle conditions and genesis of igneous pyroxenites: an experimental study. Contrib Mineral Petrol 141:643–658

Nandedkar RH, Ulmer P, Müntener O (2014) Fractional crystallization of primitive, hydrous arc magmas: an experimental study at 0.7 GPa. Contrib Mineral Petrol 167:1015, doi:10.1007/s00410-014-1015-5

Nicholls IA (1971) Petrology of Santorini Volcano, Cyclades, Greece. J Petrol 12(1):67–119

Nicholls, IA (1978) Primary basaltic magmas for the pre-Caldera volcanic rocks of Santorini. In: Doumas C (ed) Thera and the Aegean World I, pp 109–120

Oberhänsli R, Mercolli I, Dietrich VJ (1985) The amphibole andesite connection. Terra Cognita 5 (2/3):181

Oberhänsli R, Dietrich VJ, Mercolli I (1989) Origin of high-al basalts by hybridization of cumulates. Terra 1 (1):277

Osborn EF (1976) Origin of calc-alkali magma series of Santorini volcano type in the light of recent experiments phase equilibria. Proc Int Cong Therm Waters Geotherm Energy Volcanism Med Area 3:154–167

Osborn EF, Rawson SA (1980) Experimental studies of magnetite in calc-alkaline rocks. Carnegie Inst Wash Yearb 79:281–285

Pe GG (1975) Strontium isotope ratios in volcanic rocks from the northwestern part of the Hellenic Arc. Chem Geol 15:53–60

Pe-Piper G, Piper DJW (2002) The igneous rocks of Greece the anatomy of an orogen. Gebr Bornträger Berlin Stuttgart, 573 pp

Rehren Th (1988) Geochemie und Petrologie von Nisyros (Oestliche Agaeis). PhD thesis Univ Freiburg

Ridolfi F, Renzulli A, Puerini M (2010) Stability and chemical equilibrium of amphibole in calc-alkaline magmas: an overview, new thermobarometric formulations and application to subduction-related volcanoes. Contrib Mineral Petrol 160(1):45–66

Ridolfi F, Renzulli A (2012) Calcic amphiboles in calc-alkaline and alkaline magmas: thermobarometric and chemometric empirical equations valid up to 1130 °C and 22 GPa. Contrib Mineral Petrol 163:877–895

Rutherford MJ, Hill PM (1993) Magma ascent rates from amphibole breakdown: an experimental study applied to the 1980–1986 Mount St Helens eruptions. J Geophys Res B Solid Earth 98:19667–19685

Schmidt MW (1992) Phase compositions and relationships in tonalite: an experimental approach. PhD thesis ETH Zurich, Nr 9897, 113 pp

Sisson TW, Grove TL (1993a) Experimental investigations of the role of H_2O in calc-alkaline differentiation and subduction zone magmatism. Contrib Miner Petrol 113:143–166

Sisson TW, Grove TL (1993b) Temperatures and H_2O contents of low-MgO high-alumina basalts. Contrib Miner Petrol 113:167–184

Spandler C, Martin LHJ, Pettke Th (2012) Carbonate assimilation during magma evolution at Nisyros (Greece), South Aegean Arc: evidence from clinopyroxenite xenoliths. Lithos 146–147:18–33

Spear FS, Kimball KL (1984) RECAMP—A FORTRAN IV program for estimating Fe3+ contents in amphiboles. Comput Geol 10:317–325

St Seymour K, Lalonde AE (1990) Monitoring oxygen fugacity conditions in pre-, syn- and postcaldera magma chamber of Nisyros Volcano, Aegean island arc, Greece. J Volcanol Geotherm Res 46:231–240

St Seymour K, Vlassopoulos D (1989) The potential for future explosive volcanism associated with dome growth at Nisyros, Aegean Volcanic Arc, Greece. J Volcanol Geotherm Res 37:351–364

St Seymour K, Vlassopoulos D (1992) Magma mixing at Nisyros Volcano, as inferred from incompatible trace-element systematics. J Volcanol Geotherm Res 50:273–299

Stewart DC (1975) Crystal clots in calc-alkaline andesites as breakdown products of high-Al amphiboles. Contrib Miner Petrol 53(3):195–204

Sun SS, MacDonough WF (1989) Chemical and isotopic systematics of oceanic basalts: implications for mantle composition and processes. In: Saunders AD, Norry MJ (eds) Magmatism in Oceanic basins. Geol Soc Spec Publ Lond, pp 313–345

Tatsumi Y, Eggins S (1995) Subduction zone magmatism. Blackwell Scientific, Oxford

Ulmer P (2001) Partial melting in the mantle wedge—the role of H_2O in the genesis of mantle-derived 'arc-related' magmas. Phys Earth Planet Inter 127:215–232

Ulmer P, Trommsdorff V (1995) Serpentine stability to mantle depths and subduction-related magmatism. Science 268:858–861

Vanderkluysen L, Volentik A (2002) Etude géophysique et hydrothermalisme du complexe volcanique de Nisyros, Greece. Diploma thesis Univ Lausanne, 200 pp

Vanderkluysen L, Volentik A, Principe C, Hunziker JC, Hernandez J (2005) Nisyros volcanic evolution: the growth of a stratovolcano. In: Hunziker JC, Marini L (eds) The petrology and geochemistry of lavas and tephras of Nisyros Volcano (Greece). Mémoires de Géologie (Lausanne) 44:100–106

Volentik A, Vanderkluysen L, Principe C (2002) Stratigraphy of the Caldera walls of Nisyros Volcano, Greece. Eclogae Geol Helv 95:223–235

Volentik A, Vanderkluysen L, Principe C, Hunziker JC (2005) Stratigraphy of Nisyros vollcano (Greece) In: Hunziker JC, Marini L (eds) The petrology and geochemistry of lavas and tephras of Nisyros Volcano (Greece). Mémoires de Géologie (Lausanne) 44:26–66

Vougioukalakis GE (1984) Studio vulcanologico e chimico-petrografico dell'isola di Nisyros (Dodecanneso, Grecia). Università di Pisa, Tesi di laurea

Vougioukalakis G (1993) Volcanic stratigraphy and evolution of Nisyros island. Bull Geol Soc Greece 28(2):239–258

Williams H, Turner FJ, Gilbert CM (1954) Petrography. Freeman and Co, San Francisco, p 406

Wyers GP, Barton M (1989) Polybaric evolutian of calc-alkalinc magmas from Nisyros, southeastern Hellenic Arc, Greece. J Petrol 30(1):1–37

Zellmer GF, Turner SP (2007) Arc dacite genesis pathways: evidence from mafic enclaves and their hosts in Aegean lavas. Lithos 95(3–4):346–362

Zouzias K, St Seymour K (2014) Magma mixing and magma mingling episodes throughout the volcanic history of Nisyros Volcano, SE extremity of the Aegean volcanic arc, as registered by the plagioclase record. Neues Jahrbuch für Mineralogie Abhlg (J Min Geochem) 191(2):189–214